PILOT Project
Resistivity/IP Survey: Phase II

Whitehorse Mining District
NTS: 115K/09

Work Performed On: July 25th – August 4th, 2018

FOR:

White Gold Corp.
100 University Avenue, 8th Floor
Toronto, Ontario, Canada M5J 2Y1
(800) 564 6253

BY:
Jennifer Hanlon, M.Sc., GIT
GroundTruth Exploration Inc.
BOX 70, Dawson City, YT.

Date: November 4th, 2018

Table of Contents

Table of Figures

Table of Appendix Figures

1.0 Introduction

White Gold Corporation (WGO) headquartered in Toronto, ON commissioned GroundTruth Exploration Inc. (GroundTruth) headquartered in Dawson City, YT to complete high resolution resistivity and induced polarization (RES/IP) surveys on the Pilot (PLT) property during the 2018 field season.

The purpose of the RES/IP survey is to identify geological structure, trends, and to delineate extent of mineralized zones that are indicated by soil anomalies. This report details results of the RES/IP surveys conducted on PLT. Additional surveying and interpretation is left to WGO's discretion.

Figure 1 shows an overview of the proposed RES/IP survey lines to be completed within the PLT property during the 2018 field season. The figure also shows the Pilot property location in relation to Dawson City. A map of the completed grids is shown in Figure 2.

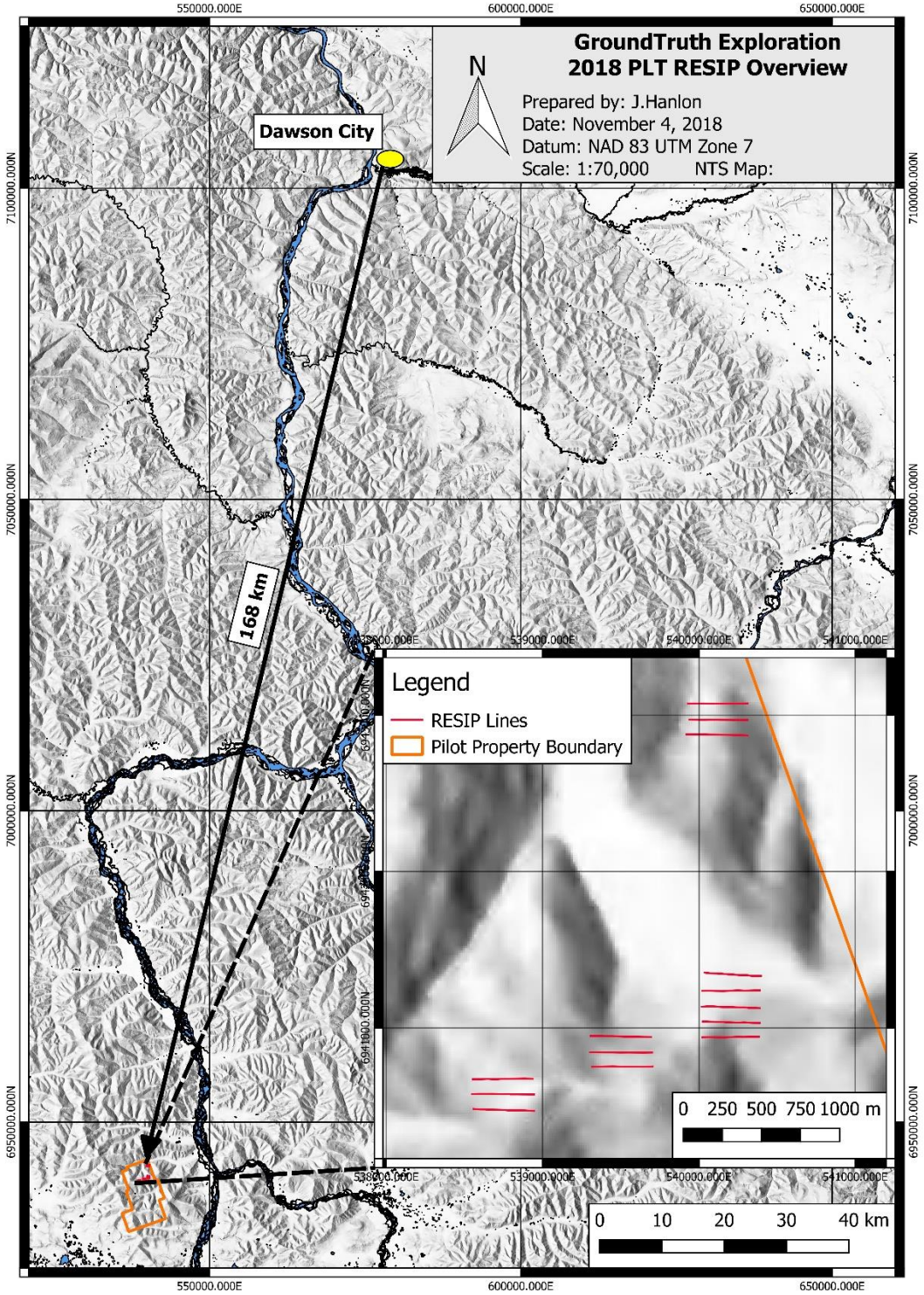

***Figure 1**: Overview map of 2018 Pilot RES/IP grids in relation to Dawson City.*

2.0 Survey Theory

Resistivity and Induced Polarization surveys are an appropriate approach to lode-source gold exploration in Yukon Territories because of the resistivity contrasts inherent to the mineralization and geological structures that are associated with gold deposits. The non-invasive nature of RES/IP combined with its cost efficiency make it a valuable contribution to exploration efforts.

RES/IP surveys involve current injection from the ground surface to induce an electric field that is a function of the conductivity distribution in the subsurface. A current injection typically uses one sink electrode and one source electrode. A measurement of potential field is then acquired across two electrodes that are different from the current electrodes. Hundreds of potential field measurements are made at intervals along the RES/IP traverse for successive current injections to generate the final raw profile of apparent subsurface resistivity.

There are a wide number of array types used to perform RES/IP surveys, each involving a different configuration of current and potential electrodes. Different arrays have strengths and weaknesses in regards to the time necessary to complete the survey and the measurement sensitivity to vertical or horizontal subsurface features. GroundTruth utilizes an extended dipole-dipole array for the Pilot project to adequately image the target zones. Details on the extended dipole-dipole array can be found in Appendix C.

2.1 Field Survey Operating Procedure

A crew of 5 GroundTruth personnel sets up and operates each survey. Brief operating procedures are as follows:

1. The midpoint of a traverse is located and the length of the line is sighted using a compass and GPS.
2. Minimal brush is cut along the line to place pickets and set up equipment.
3. 84 electrodes are diligently inserted into the ground, equivalently spaced along the line at 5m and hammered to a depth of 50cm (10% of electrode spacing).
4. Calcium Chloride (CaCl, 25% solution) is added to the base of all electrodes.
5. Cables are laid and connected to the electrodes.
6. Contact resistance test is conducted.
7. Extra electrodes and CaCl solution is added to each electrode with CR >2,000 Ohms. CR test is repeated.
8. Continue to add electrodes and CaCl until satisfactory CR values are achieved.
9. Operator initializes survey.
10. Operator uses DGPS and data collection software to document survey line parameters incl. electrode locations, topography, and notable geological/cultural features if present. Pickets are placed along the line every 50m.

11. Crew cuts and prepares the next survey line.

2.2 Data Processing

Immediately after each survey is completed in the field, the data measurements are downloaded and reviewed for integrity. Any field errors are thus addressed before moving the equipment. RES/IP datasets are processed daily by the lead operator using EarthImager2D software provided by Advanced Geosciences Inc. Outlier/noisy data are removed and the cleaned dataset is inverted. Terrain correction to the inversion mesh is applied from topographic measurements collected in the field using a differential GPS. All raw data from the DGPS and SuperSting are archived for future consultation.

2.3 Inversion

The resistivity and induced polarization data from each traverse are inverted using the processed data set in Res2dInv. The data are inverted using a smoothness-constrained inversion algorithm that utilizes a model discretized without an extended grid and using severe reduction of side block effects. After the data sets are filtered, root-mean-square measurements of iteration model-fits are assessed to determine the most adequately fitting iteration that fits the measured data without overfitting the measurement noise. An appropriate colour scale for each calculated parameter is then chosen to display the results (i.e. a logarithmic scale for resistivity and a linear scale for chargeability).

3.0 Survey Personnel and Program Dates

3.1 Survey Personnel

The following table summarizes the GroundTruth personnel involved in completing the survey lines on the Pilot property.

***Table 1**: Summary of GroundTruth personnel involved in the RES/IP data acquisition on the Pilot prospect region.*

Personnel	Position
Andrew Truax	Lead Geophysical Operator and Crew Chief
Jordan Macdonald	Secondary Lead
Joel Nevokshonoff	Geo Technician

Jason Daigle	Geo Technician
Fred D'Amours Leclerc	Geo Technician

3.2 Program Dates

Mobilize: July 25th
Field Surveys: July 26th – August 4th

Note that the field crew had remote (fly) camp accommodations on the grid site for the duration of the project, and utilized a combination of walk outs, helicopter gear-bumps, and crew set outs to maximize time and cost efficiency of surveying each of the four grids.

4.0 Survey Summary

An overview of the RES/IP grid on the Pilot property is shown in Figure 2. Brief specifications about the survey lines are outlined below.

Lines:	PLTIP18-01 – PLTIP18-14
Number of Electrodes	84
Electrode Spacing	5m
Line Length	415m
Array	Extended dipole-dipole

The four RES/IP grids are located on the northern end of the Pilot quartz claim. Grid 2, 3, and 4 are adjacent to each other over a small ridge that trends E-W and grid 1 is about 2 km north of grids 2, 3, and 4 down a spur line. All grid lines have a bearing of 90 degrees (E-W).

The grids are covered by mostly thick vegetation composed of a variety of spruce and poplar trees. Ground is rocky in areas but mostly soil-rich and covered by moss or low lying vegetation. RES/IP lines that traverse through areas with dense roots or rocks have a larger range in electrode contact resistance, up to 11,000 Ohms. In general, contact resistances ranged between 1,000–4,500 Ohms for each of the lines, which ensures relatively stable resistance readings considering the power capability of the SuperSting.

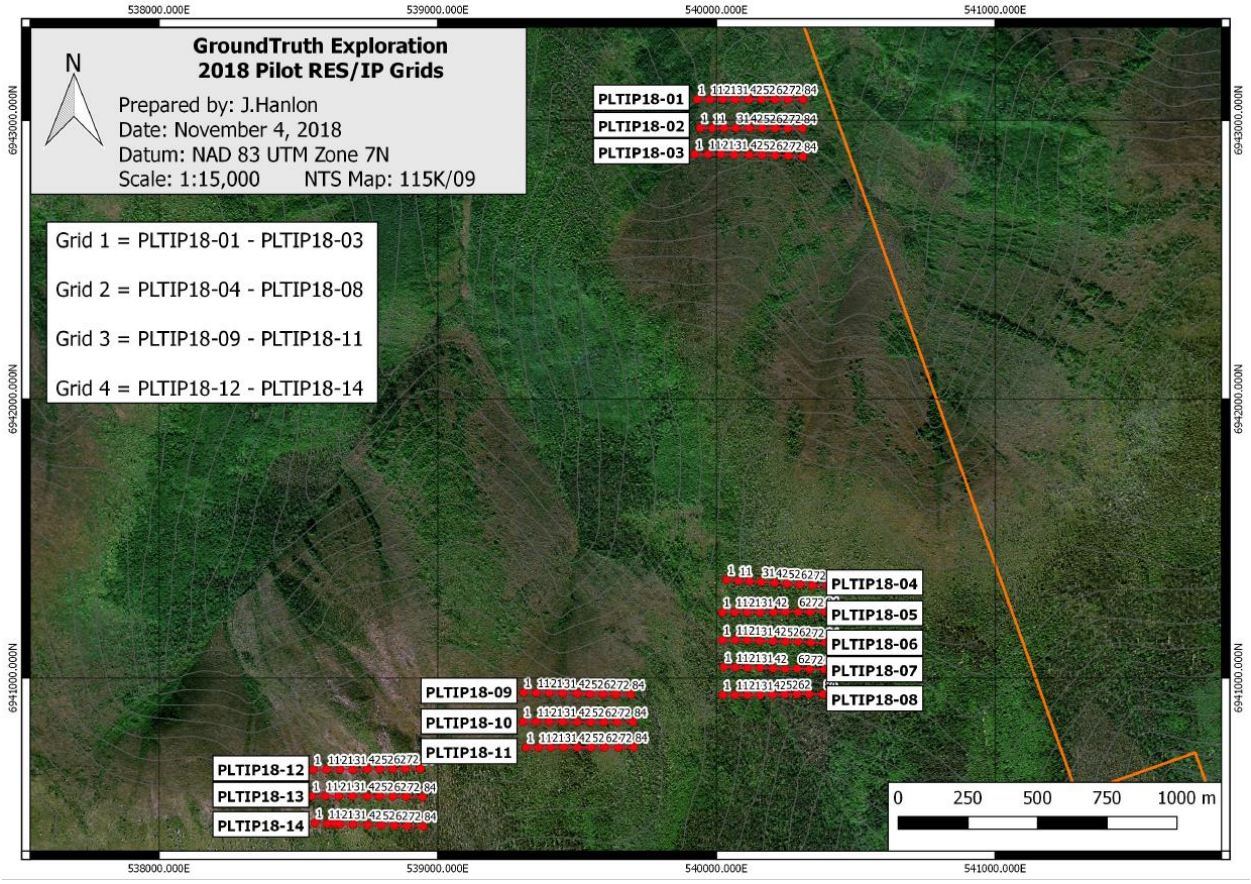

***Figure 2**: 2018 completed RES/IP grids on the Pilot property.*

5.0 Survey Results

The following figures display the inverted resistivity and induced polarization results along each traverse on the Pilot property in 2018. Note that the depth of penetration of the IP results is generally less than the resistivity results. Figures 17-20 show pseudo 2.5-D visualizations of the RES/IP inversion results over each grid. Note that in these figures that the end points of each survey are georeferenced in the final image.

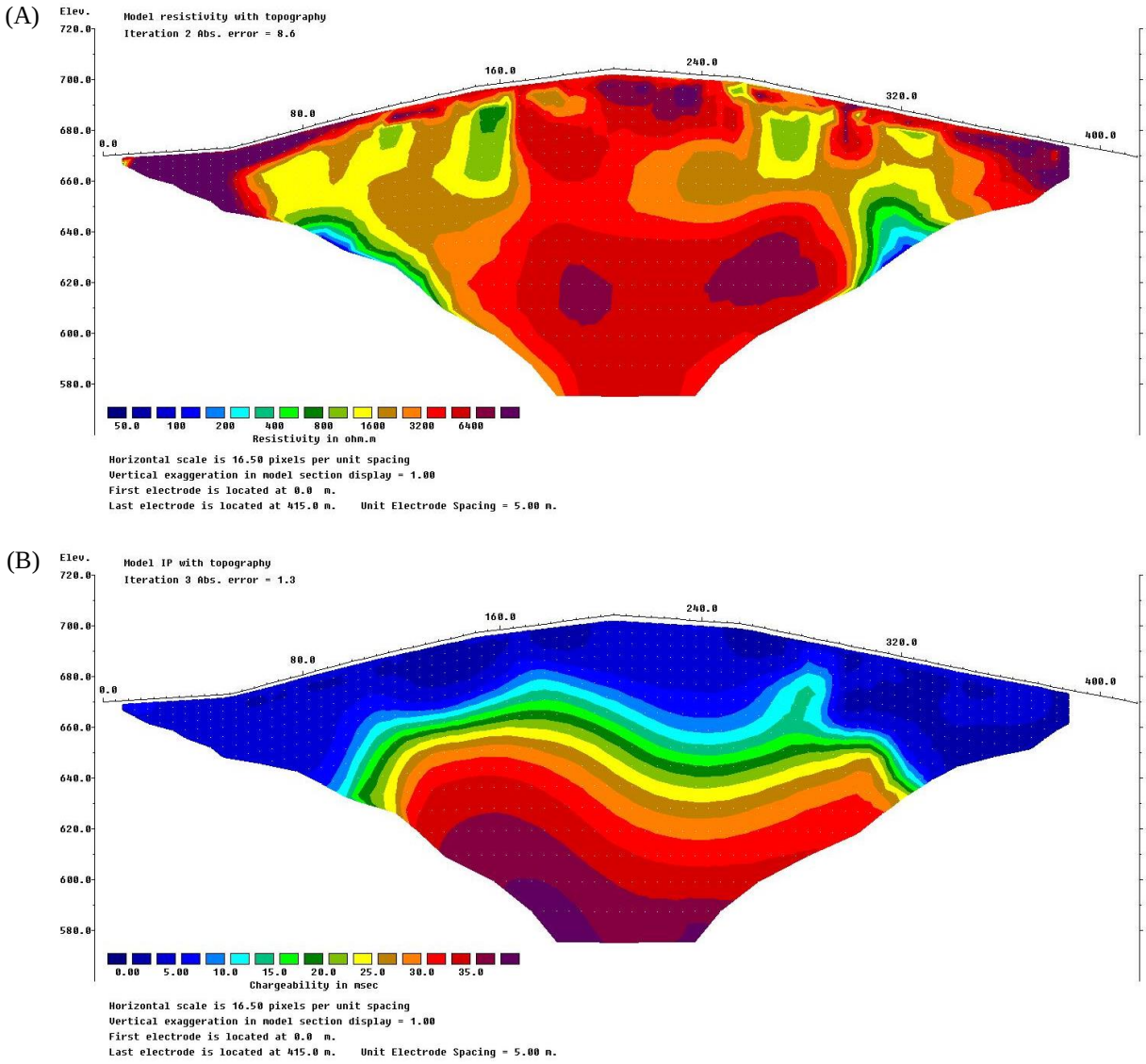

***Figure 3**: PLTIP18-01 sections. (**A**) Inverted resistivity (scale 0-9050 Ohm-m). (**B**) Inverted IP (scale 0-40 ms).*

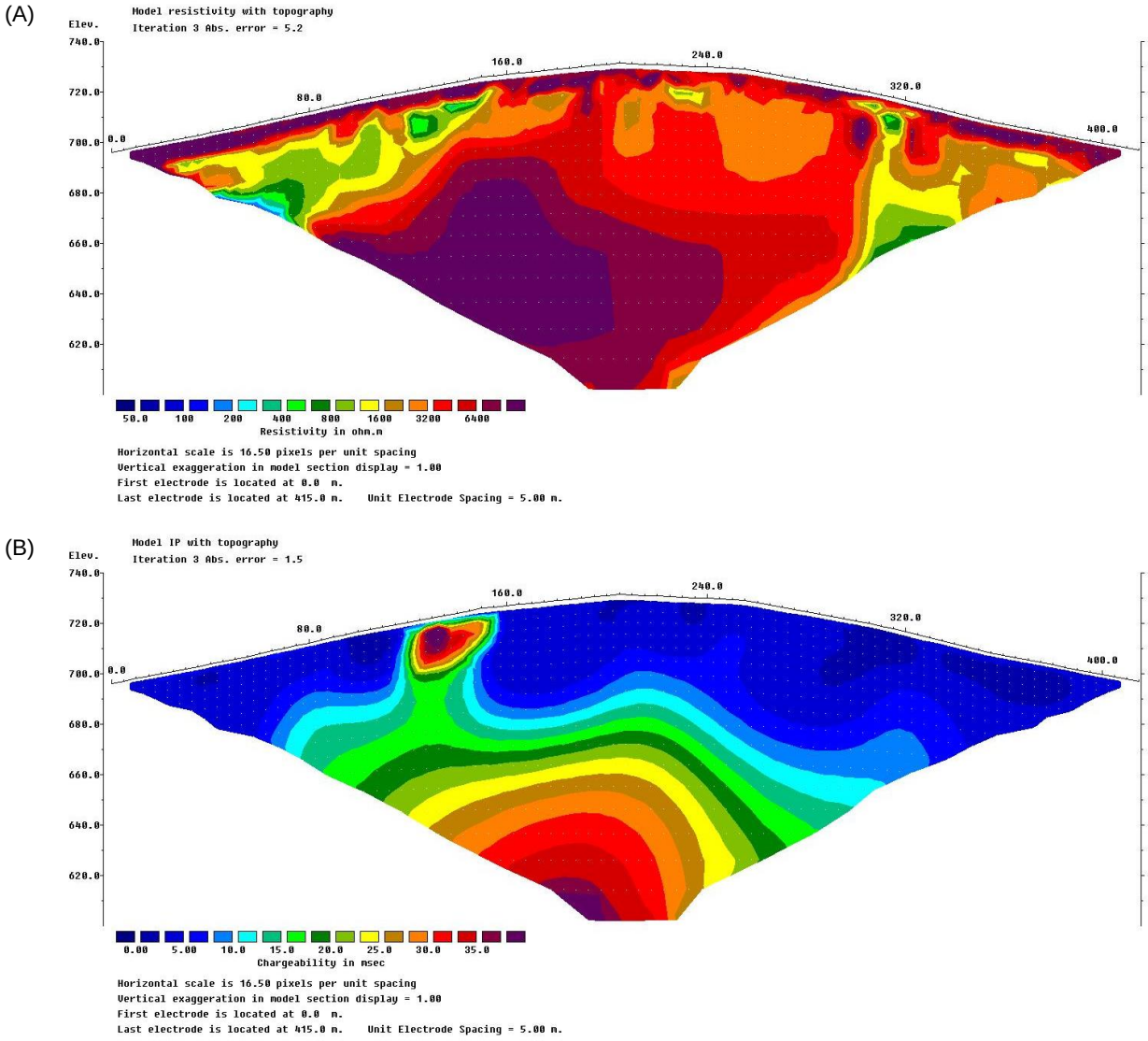

***Figure 4**: PLTIP18-02 sections. (**A**) Inverted resistivity (scale 0-9050 Ohm-m). (**B**) Inverted IP (scale 0-40 ms).*

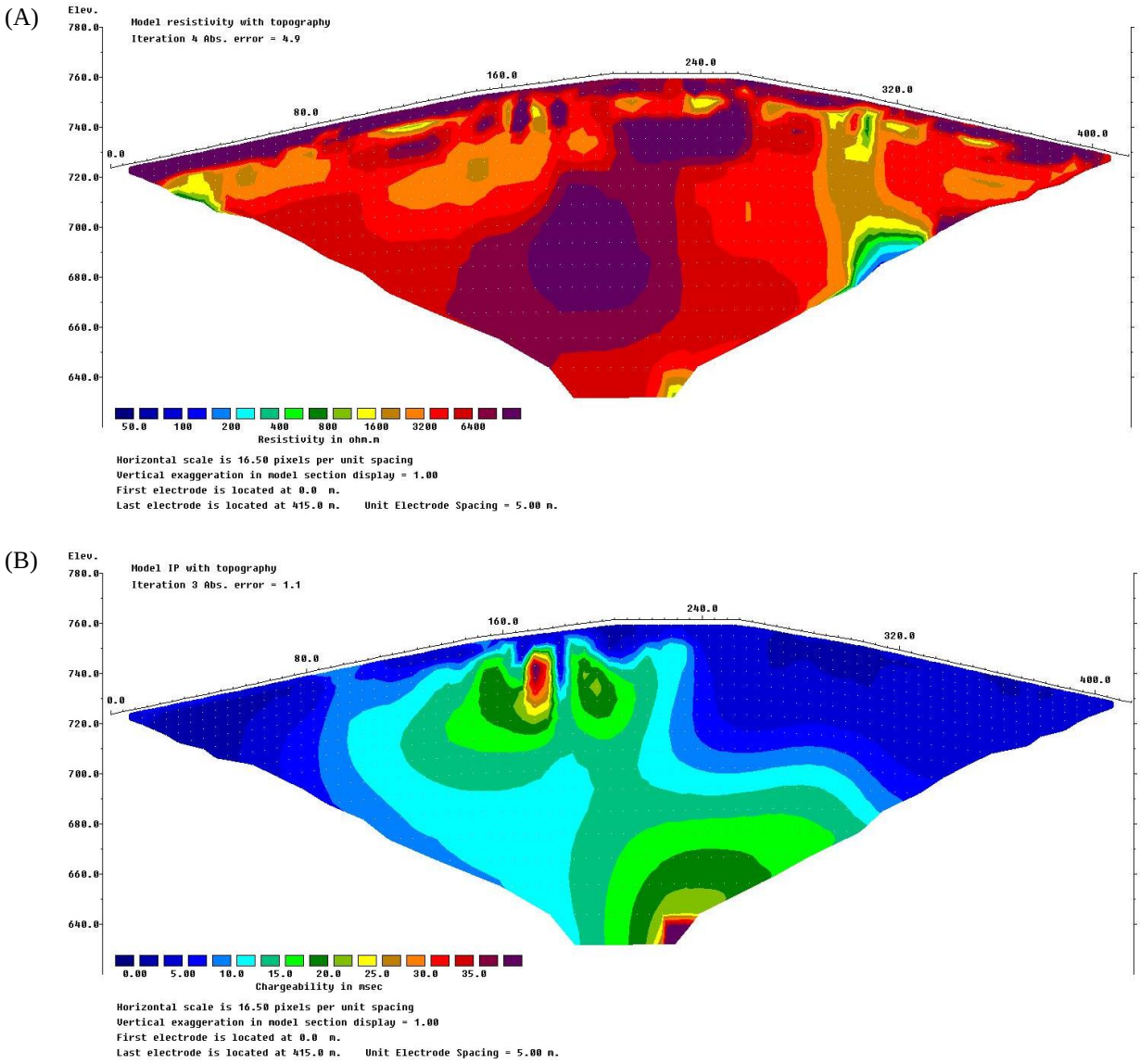

***Figure 5**: PLTIP18-03 sections. (**A**) Inverted resistivity (scale 0-9050 Ohm-m). (**B**) Inverted IP (scale 0-40 ms).*

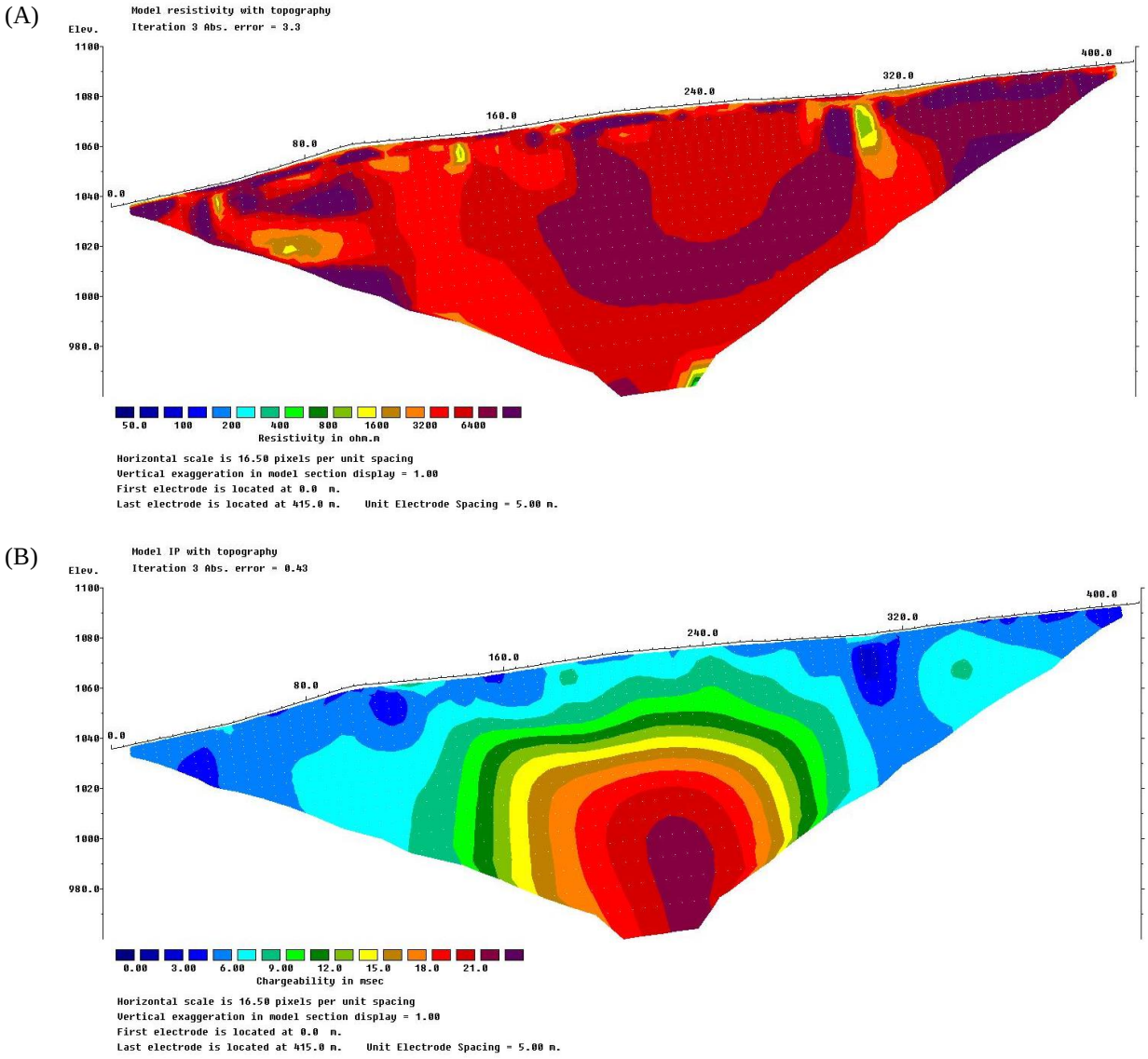

***Figure 6**: PLTIP18-04 sections. (**A**) Inverted resistivity (scale 0-9050 Ohm-m). (**B**) Inverted IP (scale 0-24 ms).*

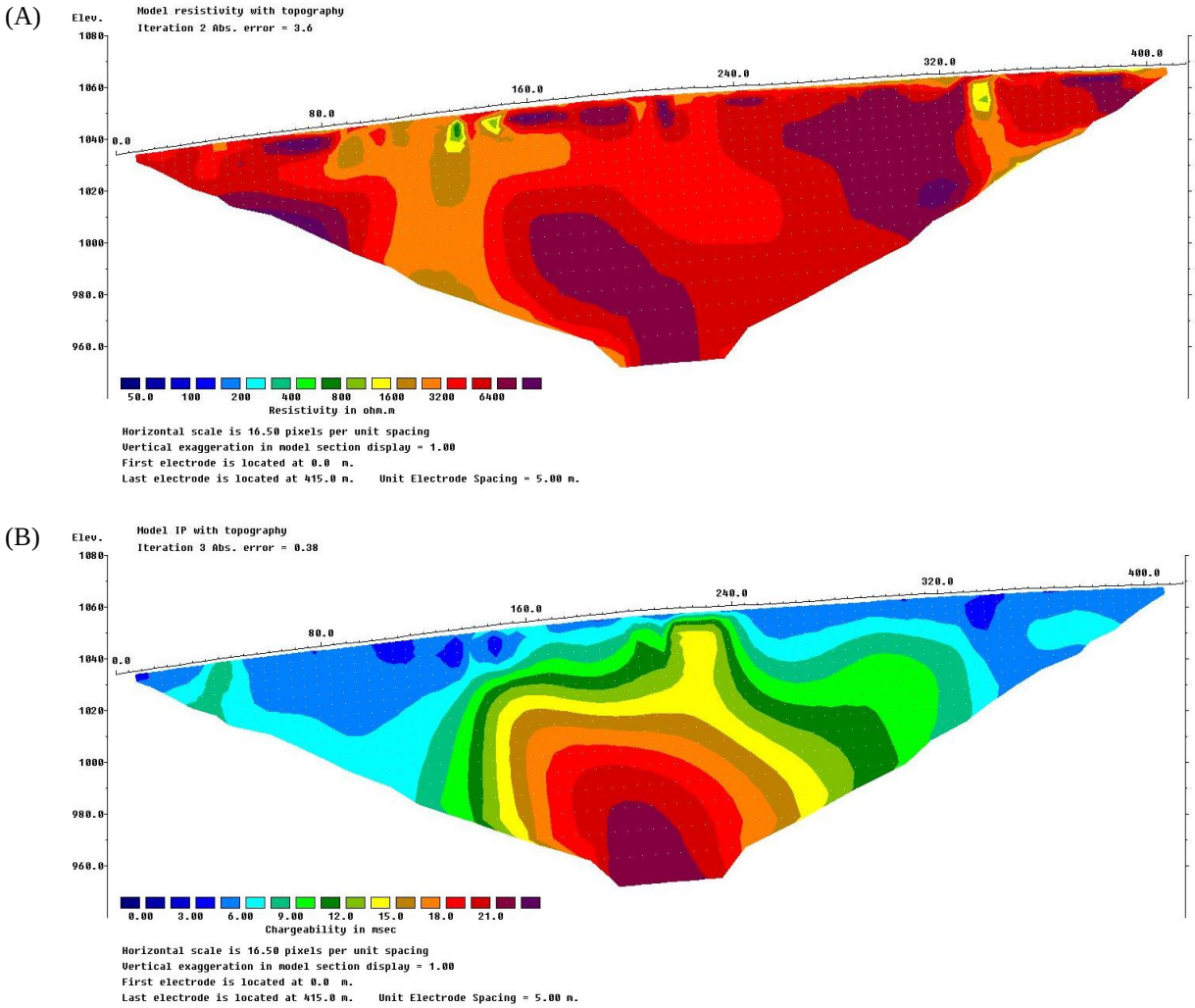

***Figure 7**: PLTIP18-05 sections. (**A**) Inverted resistivity (scale 0-9050 Ohm-m). (**B**) Inverted IP (scale 0-24 ms).*

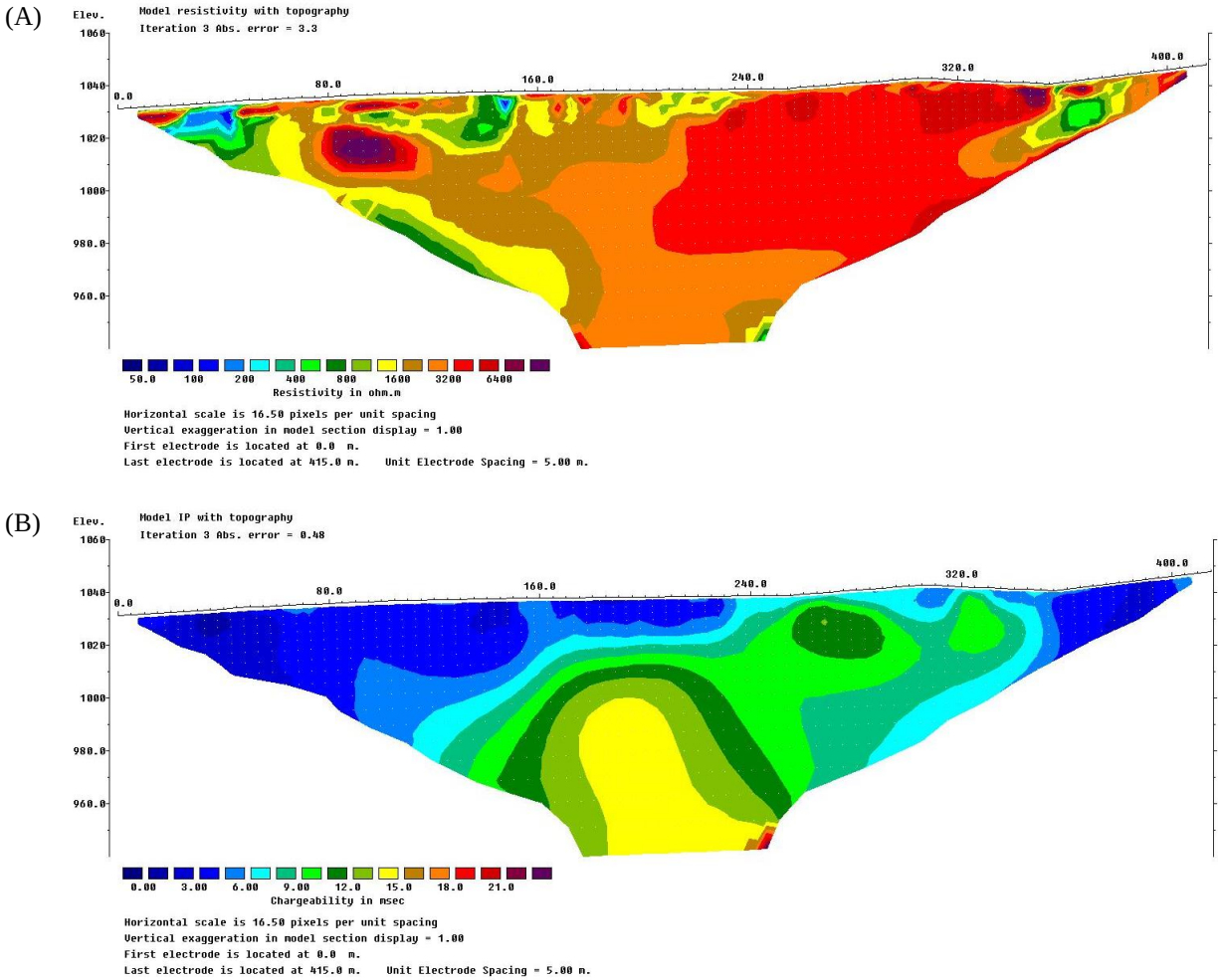

***Figure 8**: PLTIP18-06 sections. (**A**) Inverted resistivity (scale 0-9050 Ohm-m). (**B**) Inverted IP (scale 0-24 ms).*

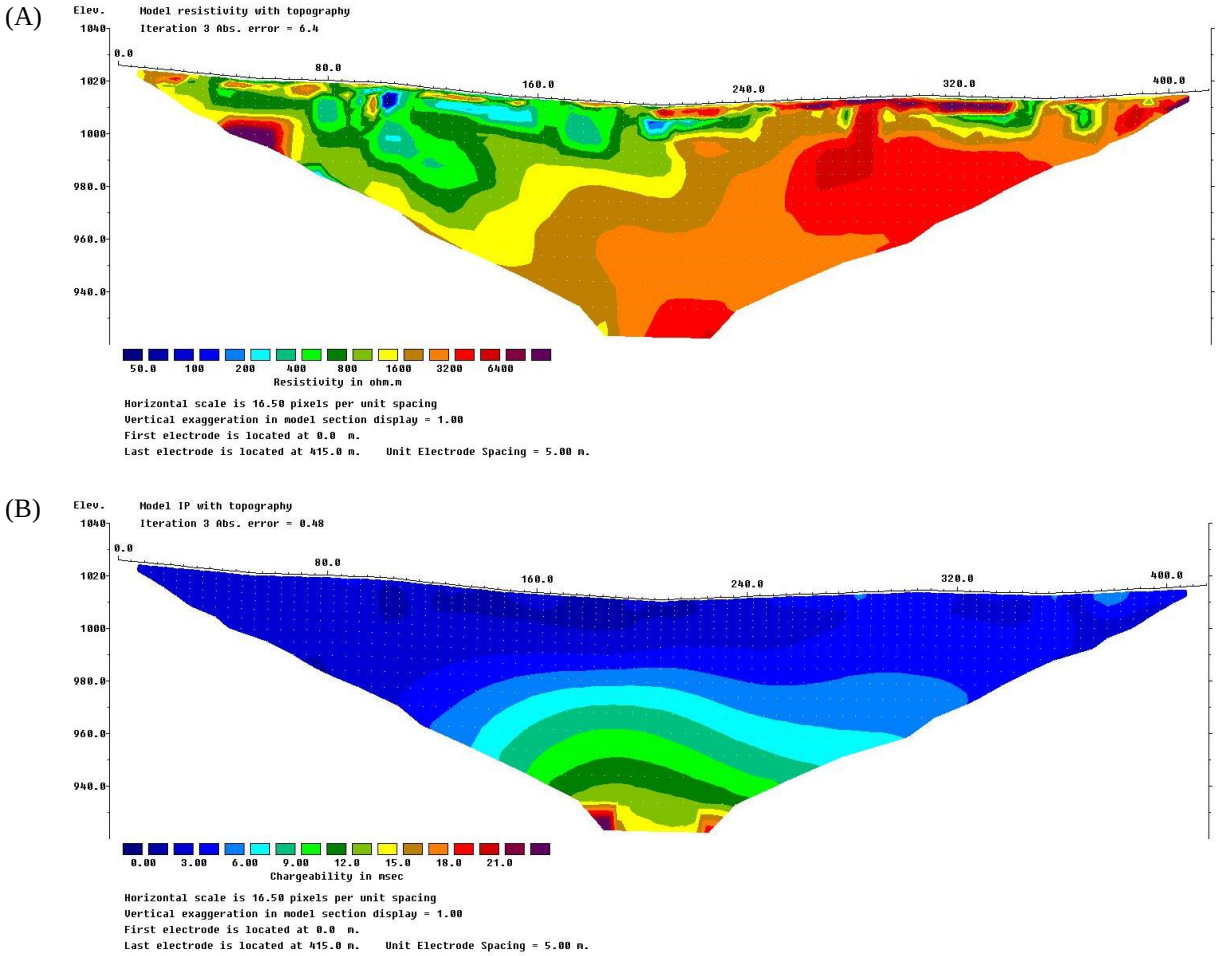

***Figure 9**: PLTIP18-07 sections. (**A**) Inverted resistivity (scale 0-9050 Ohm-m). (**B**) Inverted IP (scale 0-24 ms).*

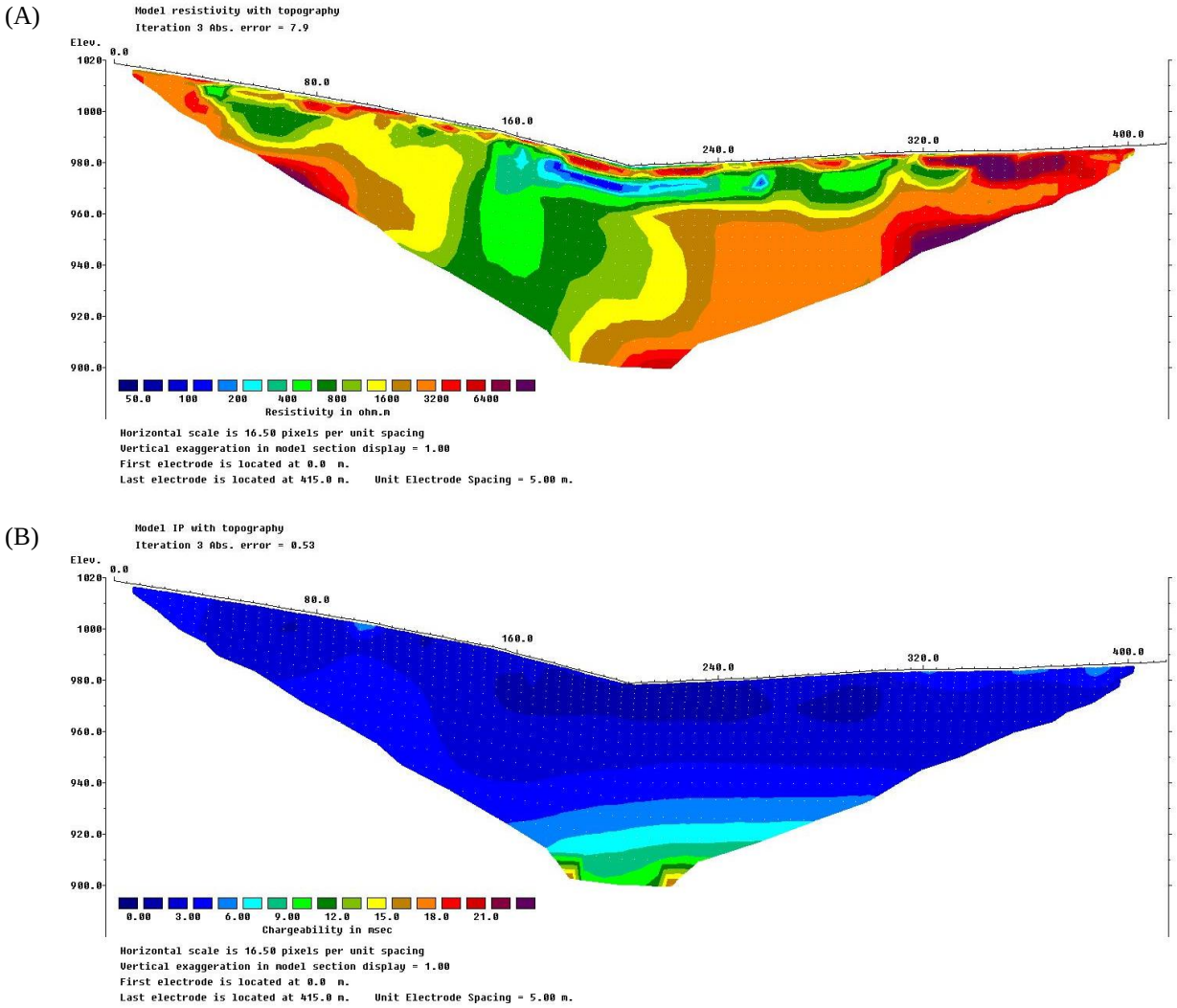

***Figure 10**: PLTIP18-08 sections. (**A**) Inverted resistivity (scale 0-9050 Ohm-m). (**B**) Inverted IP (scale 0-24 ms).*

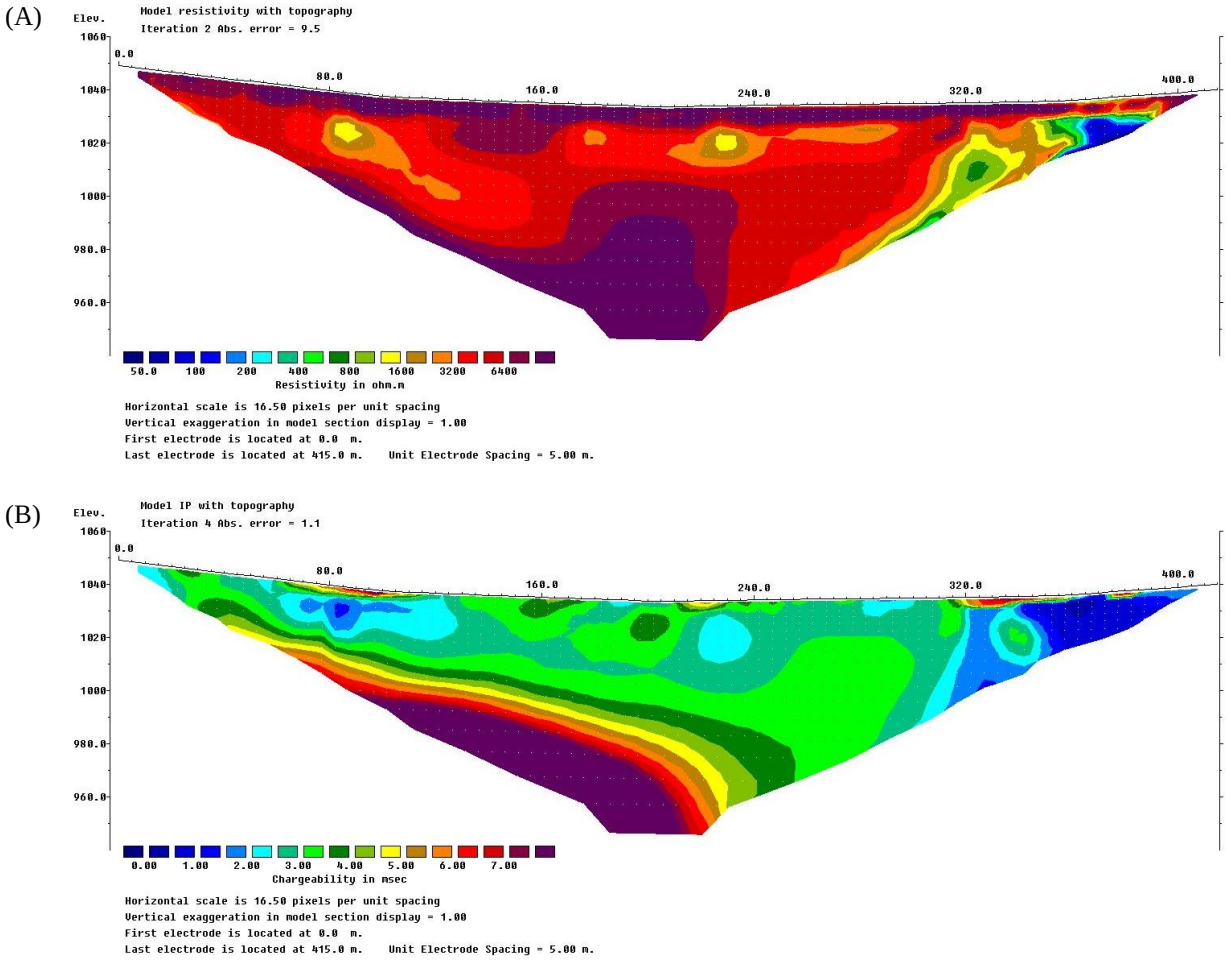

***Figure 11**: PLTIP18-09 sections. (**A**) Inverted resistivity (scale 0-9050 Ohm-m). (**B**) Inverted IP (scale 0-7.5 ms).*

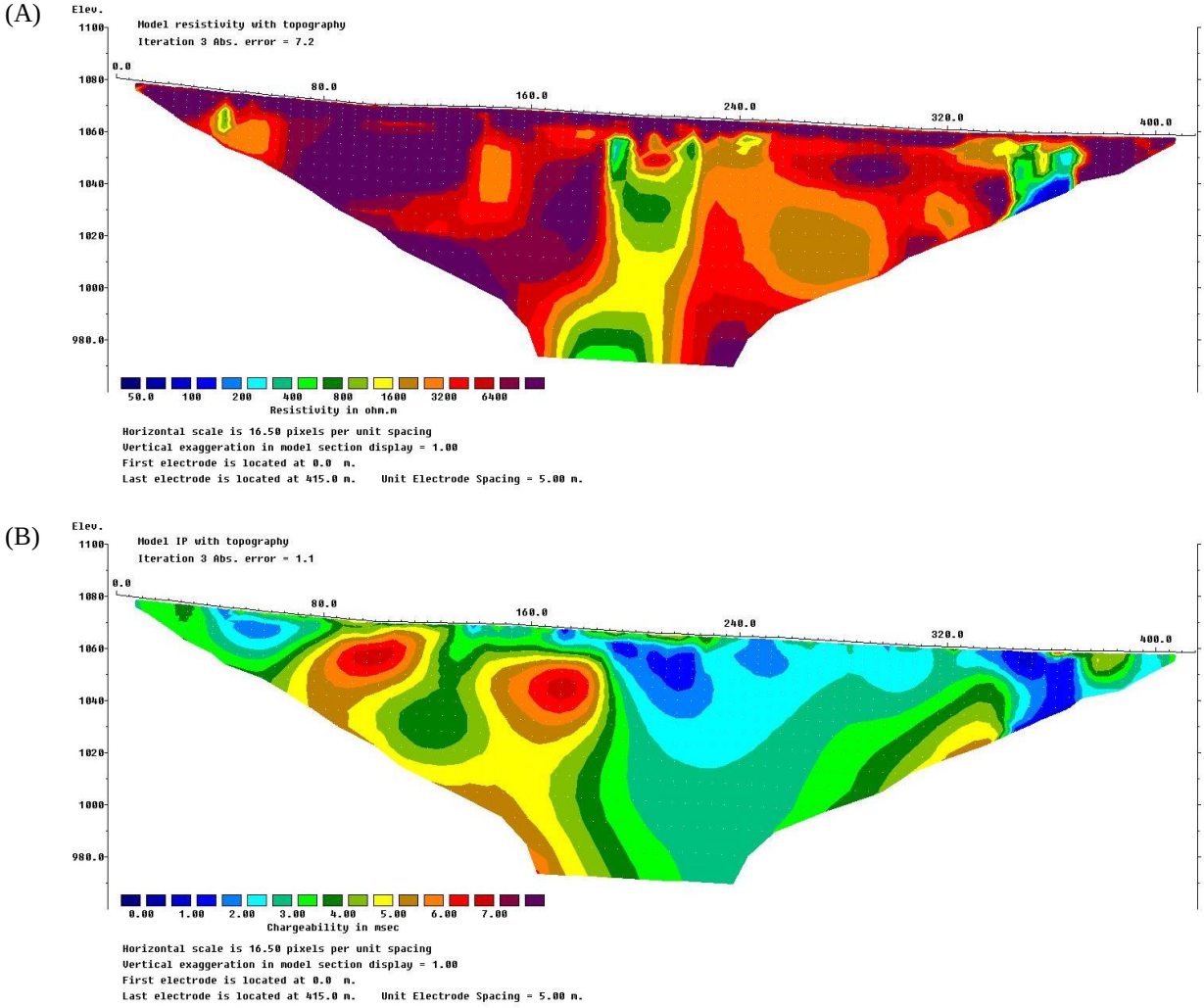

***Figure 12**: PLTIP18-10 sections. (**A**) Inverted resistivity (scale 0-9050 Ohm-m). (**B**) Inverted IP (scale 0-7.5 ms).*

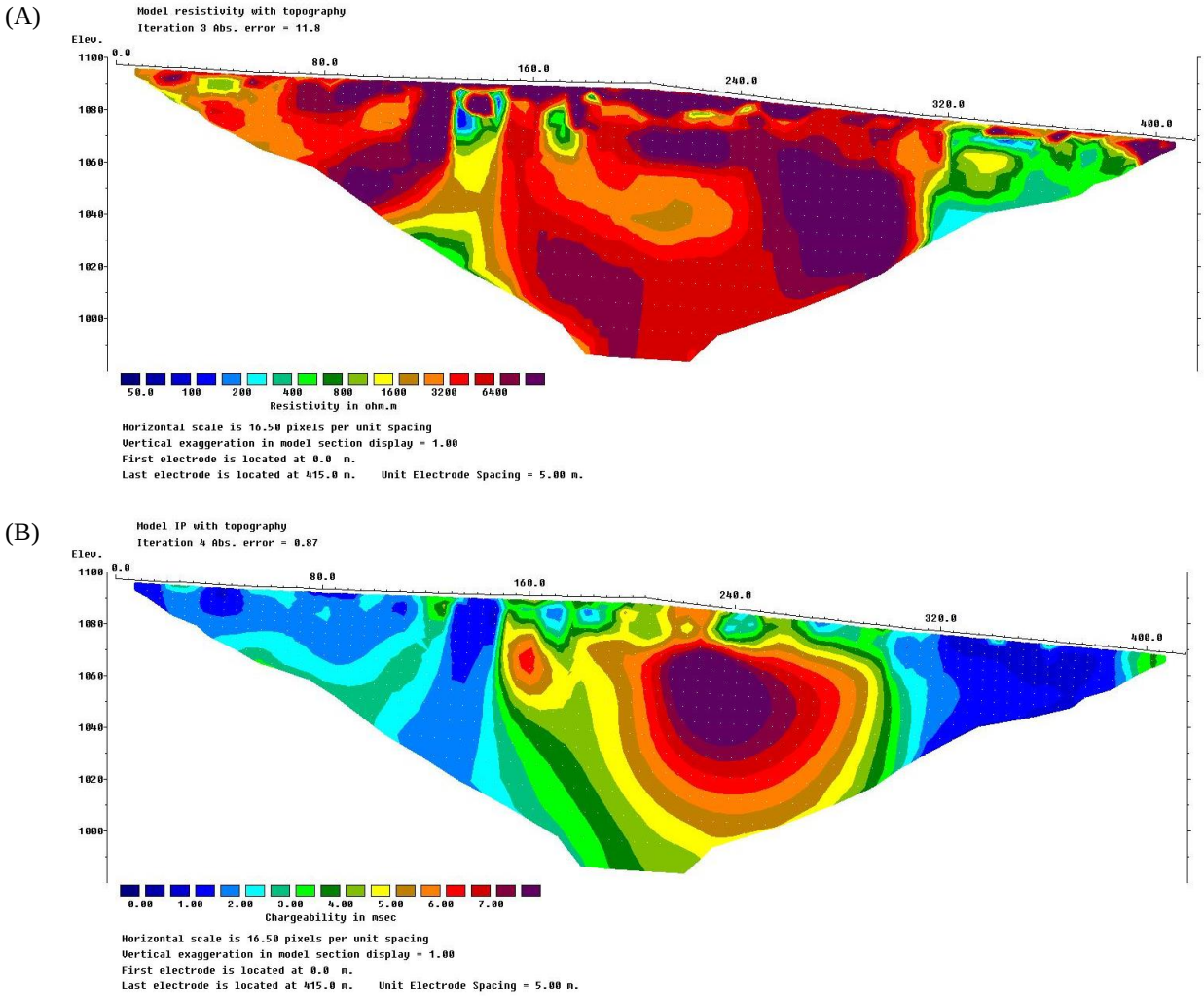

***Figure 13**: PLTIP18-11 sections. (**A**) Inverted resistivity (scale 0-9050 Ohm-m). (**B**) Inverted IP (scale 0-7.5 ms).*

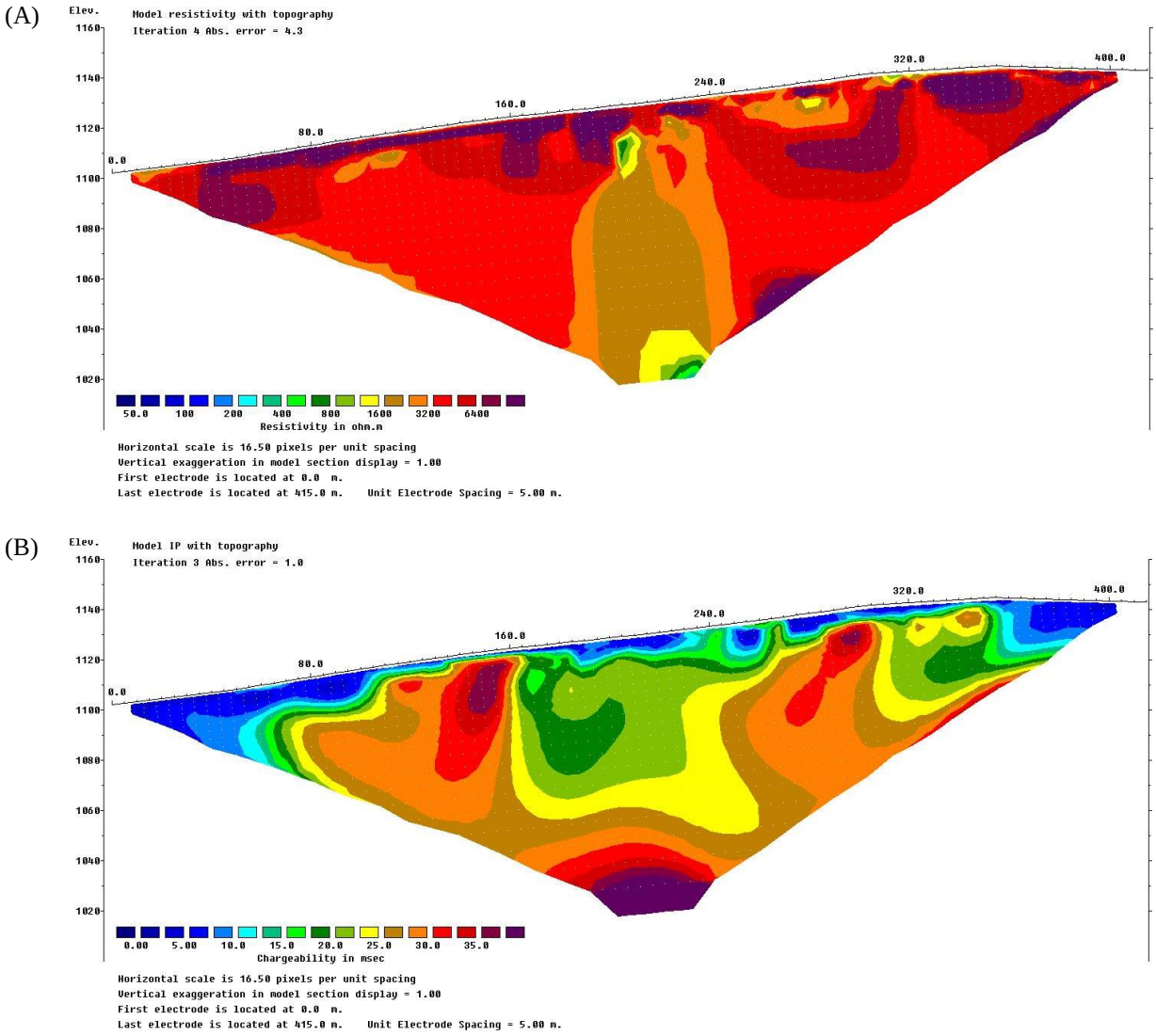

***Figure 14**: PLTIP18-12 sections. (**A**) Inverted resistivity (scale 0-9050 Ohm-m). (**B**) Inverted IP (scale 0-40 ms).*

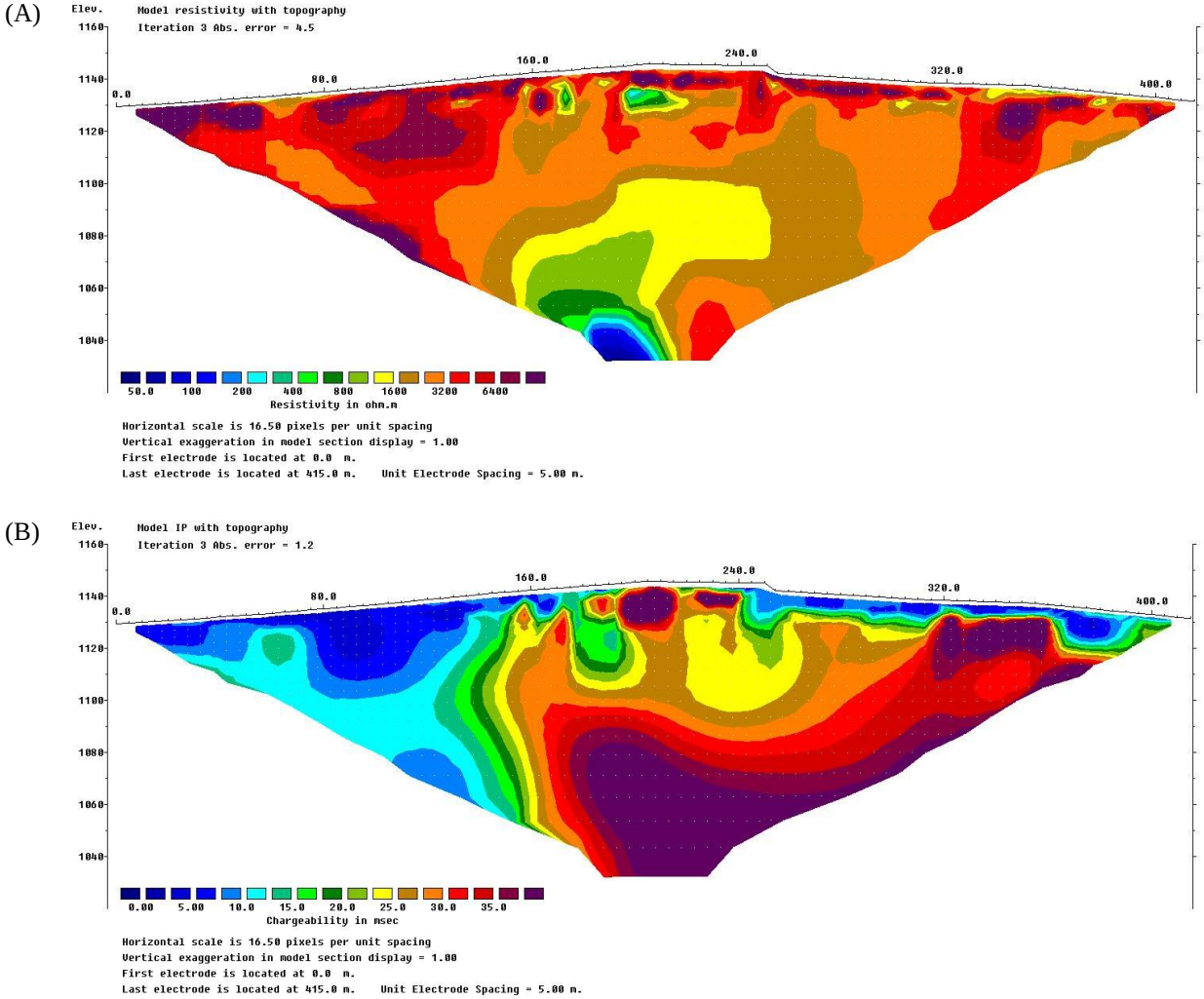

***Figure 15**: PLTIP18-13 sections. (**A**) Inverted resistivity (scale 0-9050 Ohm-m). (**B**) Inverted IP (scale 0-40 ms).*

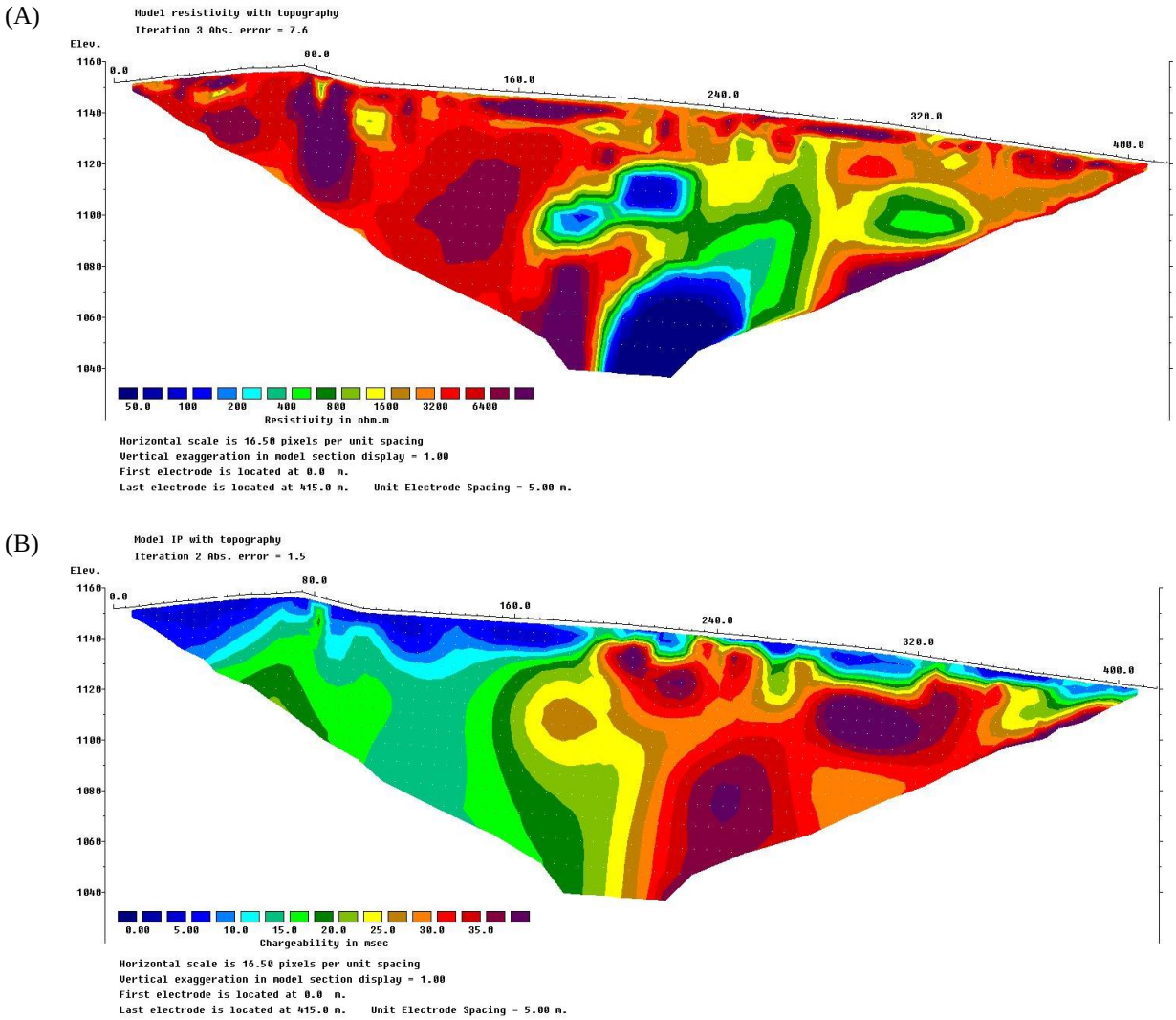

***Figure 16**: PLTIP18-14 sections. (**A**) Inverted resistivity (scale 0-9050 Ohm-m). (**B**) Inverted IP (scale 0-40 ms).*

(A)

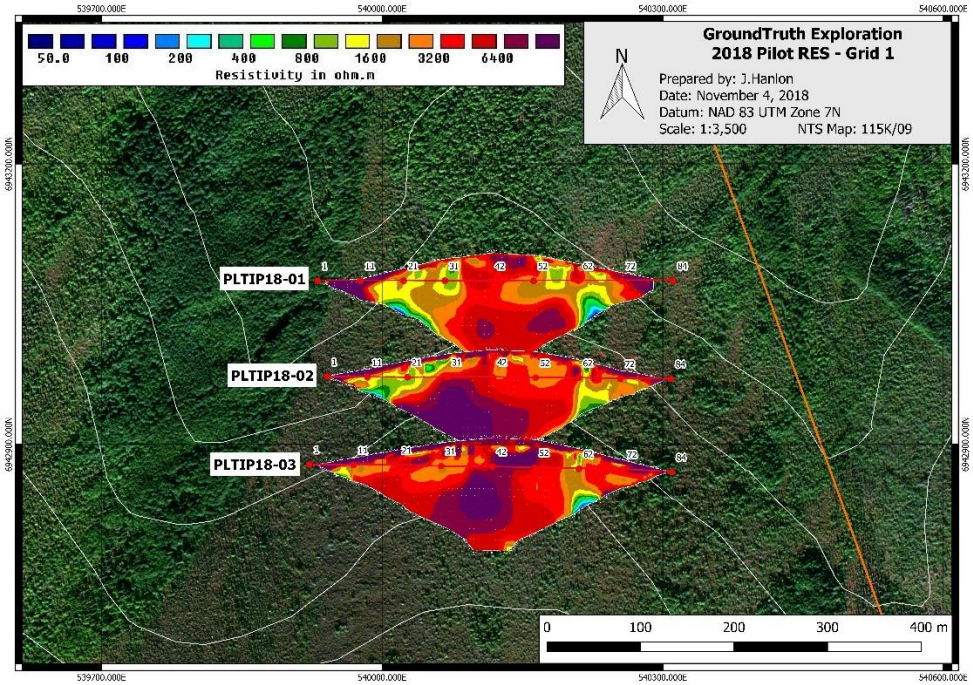

(B)

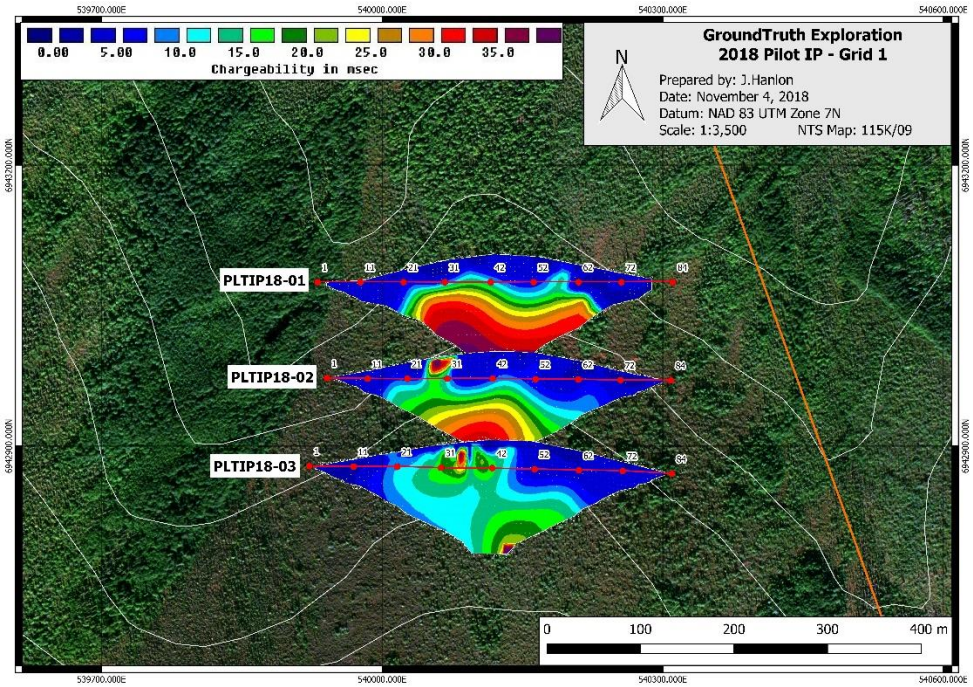

***Figure 17**: Pseudo 2.5-D visualization of inversion results on the Pilot Grid 1. (**A**) Resistivity. (**B**) Chargeability. Note that the endpoints of each line are the only georeferenced points in the image.*

(A)

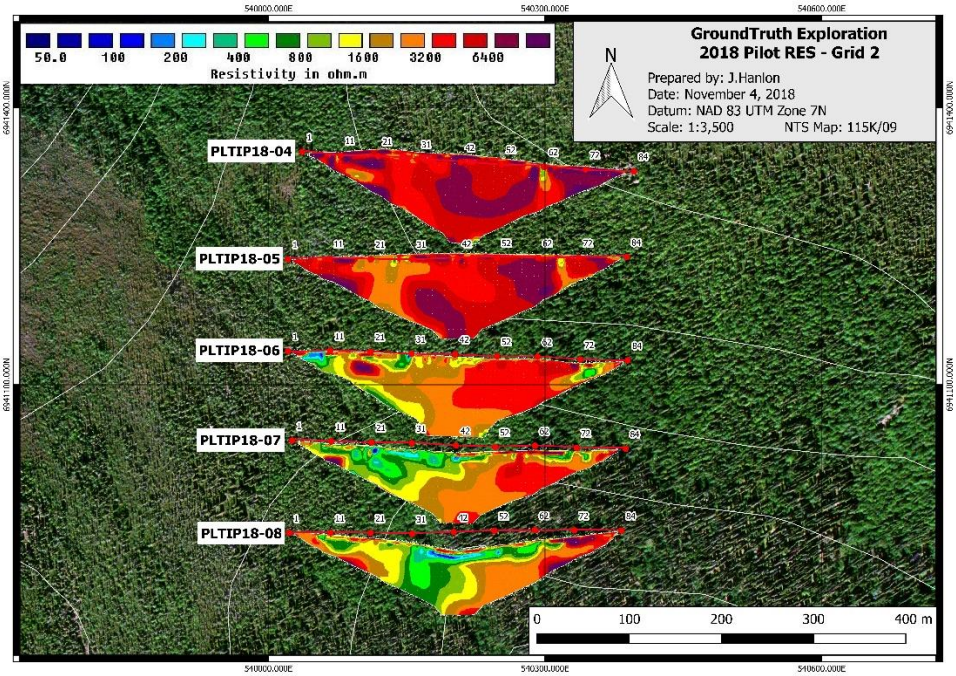

(B)

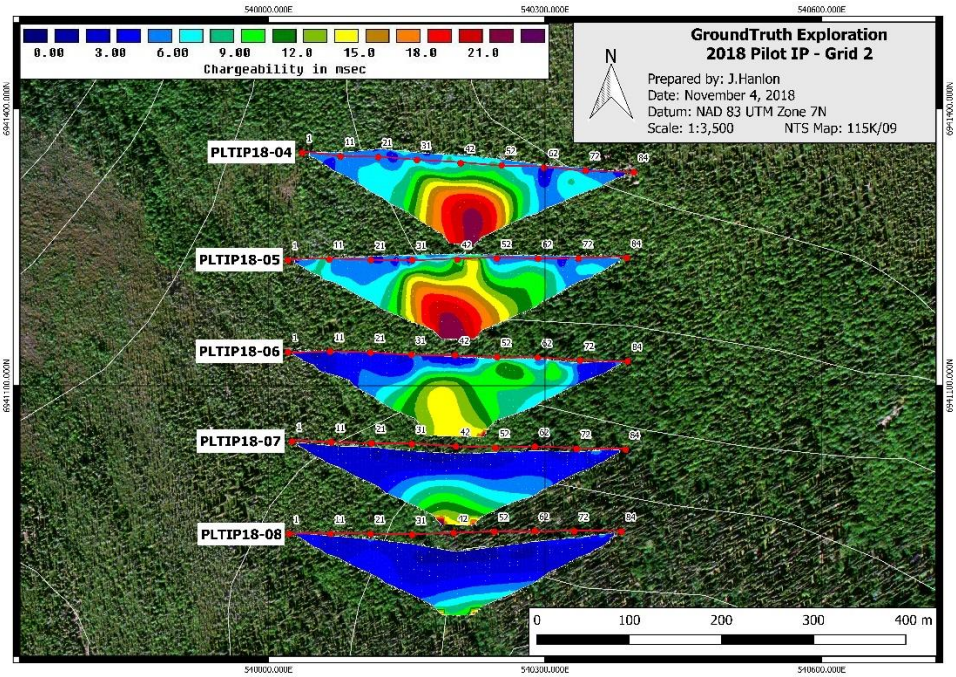

***Figure 18**: Pseudo 2.5-D visualization of inversion results on the Pilot Grid 2. (**A**) Resistivity. (**B**) Chargeability. Note that the endpoints of each line are the only georeferenced points in the image.*

(A)

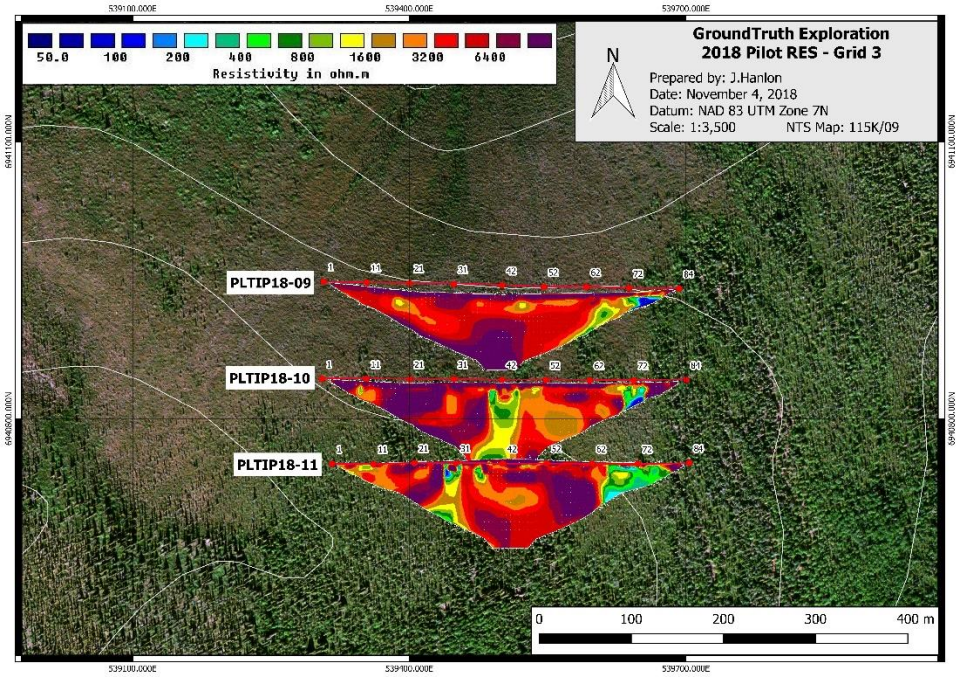

(B)

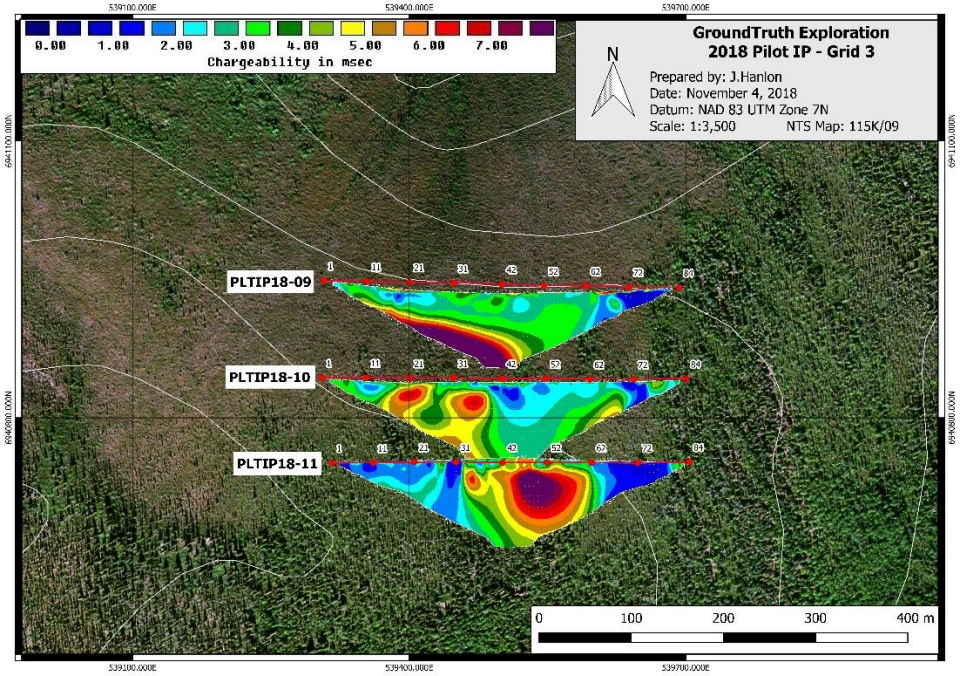

***Figure 19**: Pseudo 2.5-D visualization of inversion results on the Pilot Grid 3. (**A**) Resistivity. (**B**) Chargeability. Note that the endpoints of each line are the only georeferenced points in the image.*

(A)

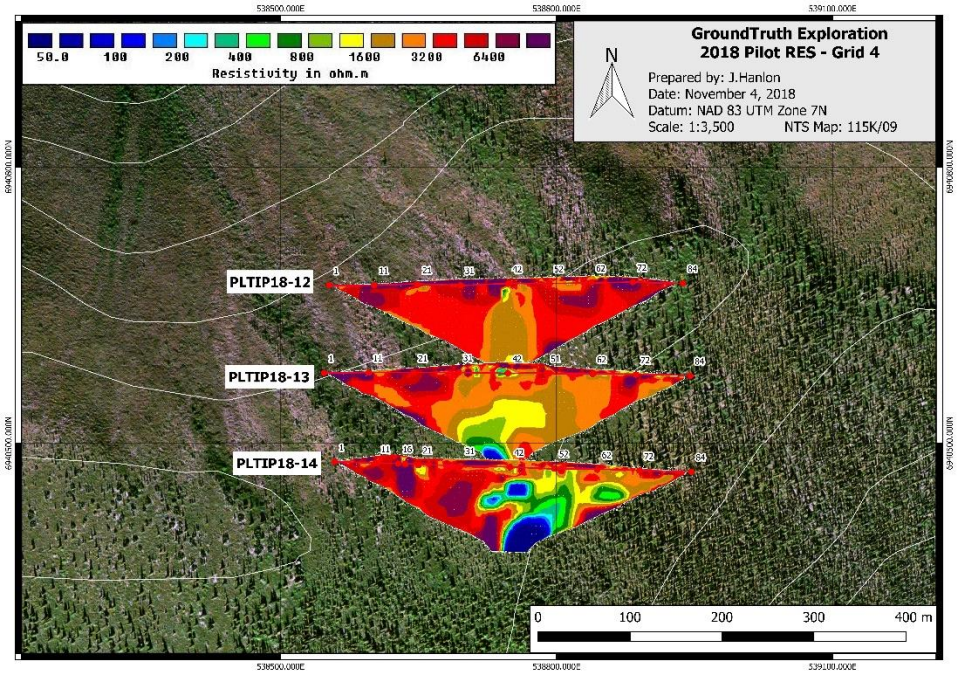

(B)

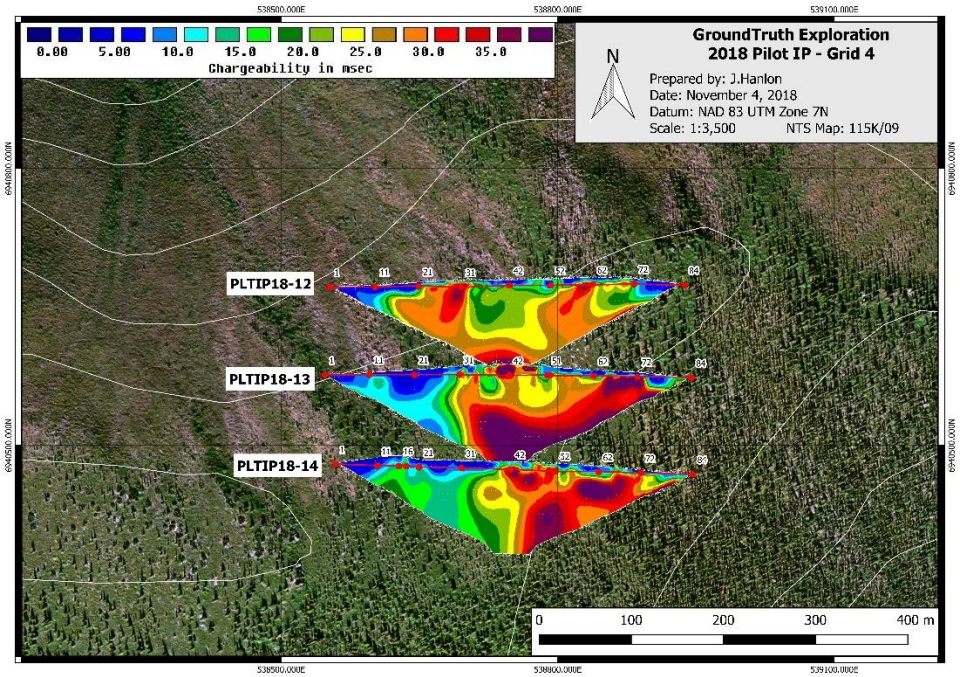

***Figure 20**: Pseudo 2.5-D visualization of inversion results on the Pilot Grid 4. (**A**) Resistivity. (**B**) Chargeability. Note that the endpoints of each line are the only georeferenced points in the image.*

6.0 Interpretation

Interpretation of 2-D resistivity and induced polarization surveys first requires identifying anomalous zones that are caused by real subsurface electrical boundaries versus those that are artefacts formed during the inversion process. This section provides a brief qualitative description of the electrical conductivity and chargeability anomalies that trend between the RES/IP sections presented in section 5.0.

Using a coarse representation map of Yukon bedrock geology (Figure 21), the Pilot grids are situated on metamorphosed bedrock Paleozoic - Ordovician in age that is composed of quartzite, micaceous quartzite, psammitic quartz-muscovite-biotite with intermittent garnet schist. There is a relatively small exposure of hornblende gabbro and pyroxenite sills to the west, and a large zone of hornblende-biotite granodiorite, hornblende diorite, quartz diorite, and quartz monzonite to the east. The resistivity sections show mostly N-S trends in conductivity in each of the grids (with the exception of grid 2, which appears to be NW-SE, and grid 3, which is NE-SW). The bulk of the subsurface has a resistivity between 3,000-7,000 Ohm-m, which is typical of metamorphic rocks.

The chargeability sections again show N-S trends at depth in grids 1 and 2. Grid 3 shows a NW-SE trend, and grid 4 shows a more chargeable unit on the east side of the grid that trends mostly N-S and forks off in PLTIP18-09.

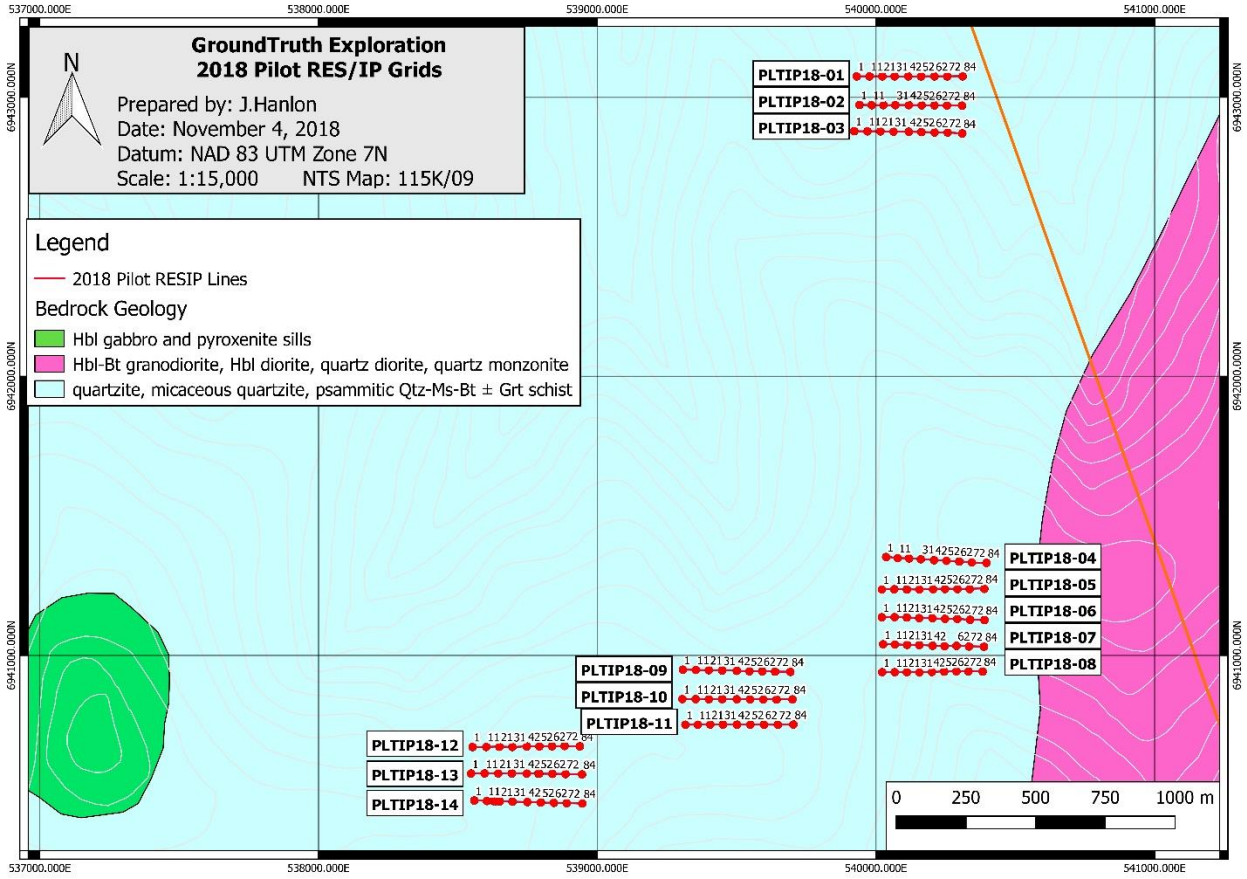

Figure 21: Regional bedrock geology.

Appendix A: Description of Files and File Structure

This section explains the file naming structure and data content for each project.

Each RES/IP traverse has a unique **Line ID** created by combining: (1) the three letter project code for the property or zone, (2) an IP or RES data designation, (3) the last two digits of the year the survey was read, and (4) an identifying number for the traverse within each property or zone.

> Example: ALBIP17-01, where ALB is the project code, IP is the type of data collected, 17 represents the year 2017, and 01 means that this is the first RES/IP dataset acquired on this property.

Each array dataset has a unique **Data File ID**. This ID is comprised by the date (yy-mm-dd), the first letter of the array type used (e.g. D for dipole-dipole or W for Wenner), and the number of times this array has been used that day.

> Example: 170813D1

File Structure and Content:

- DATA
  - Line ID
    - **Figures**
      - figures of merged data pseudosections and inversions
    - **GPS**
      - Contains the DGPS raw data
    - **Pictures**
      - Pictures along the line
    - **RAW**
      - **IP** (data with IP data-misfits removed)
      - **RES** (data with RES data-misfits removed)
      - unprocessed data from SuperSting unit
    - **XYZ**
      - Inverted data for RES and IP saved in XYZ format

Appendix B: SuperSting R1/IP technical specification

Measurement modes	Apparent resistivity, resistance, self potential (SP), induced polarization (IP), battery voltage
Measurement range	+/- 10V
Measuring resolution	Max 30 nV, depends on voltage level
Screen resolution	4 digits in engineering notation
Output current	1mA – 2 A continuous, measured to high accuracy
Output voltage	800 Vp-p, actual electrode voltage depends on transmitted current and ground resistivity
Output power	200 W
Input gain ranging	Automatic, always uses full dynamic range of receiver
Input impedance	>20 MΩ
SP compensation	Automatic cancellation of SP voltages during resistivity measurement. Constant and linearly varying SP cancels completely.
Type of IP measurement	Time domain chargability (M), six time slots measured and stored in memory
IP current transmission	ON+, OFF, ON-, OFF
IP time cycles	0.5, 1 , 2 , 4 and 8 seconds (combined resistivity/IP mode)
Measure cycles	Running average of measurement displayed after each cycle. Automatic cycle stop when reading errors fall below user set limit or user set max cycles are done.
Resistivity time cycles	Basic measure time is 0.4, 0.8, 1.2, 3.6, 7.2 or 14.4 seconds as selected by user via keyboard, autoranging and commutation adds about 1.4 s.
Signal processing	Continuous averaging after each complete cycle. Noise errors calculated and displayed as percentage of reading. Reading displayed as resistance (ΔV/I) and apparent resistivity (Ωm). Resistivity is calculated using user entered electrode array coordinates.
Noise suppression	Better than 100 dB at f>20 Hz Better than 120 dB at power line frequencies (16 2/3, 20, 50 and 60 Hz) for measure cycles of 1.2 s and above
Total accuracy	Better than 1% of reading in most cases (lab measurements). Field measurement accuracy depends on ground noise and resistivity. Instrument will calculate and display running estimate of measuring accuracy.
System calibration	Calibration is done digitally by the microprocessor based on correction values stored in memory.
Supported manual	Resistance, Schlumberger, Wenner, dipole-dipole, pole-dipole, pole-pole, SP-absolute, SP-gradient

Operating system	Stored in re-programmable flash memory. New version can be downloaded from our web site and stored in the flash memory.
Data storage	Full resolution reading average and error are stored along with user entered coordinates and time of day for each measurement. Storage is effected automatically in a job oriented file system
Data display	Apparent resistivity (Ohmmeter), injected current (mAmp) and measured voltage (mVolt) are displayed and stored in memory for each measurement
Memory capacity	The memory can store 24,468 measurements in Resistivity Mode and 14,966 measurements in combined Resistivity/IP Mode
Data transmission	RS-232C channel available to dump data from the instrument to a Windows type computer on user command.
Automatic multi-electrodes	The SuperSting is designed to run dipole-dipole, pole-dipole, pole-pole, Wenner and Schlumberger surveys including roll-along surveys completely automatic with the Swift Dual Mode Automatic Multi-electrode system (patent 6,404,203) or with switch box and passive cables. The SuperSting can run any other array by using user programmed command files. These files are ASCII files and can be created using a regular text editor. The command files are downloaded to the SuperSting RAM memory and can at any time be recalled and run. Therefore there is no need for a fragile computer in the field.
Manual measurements	The instrument has four banana pole screws for connecting current and potential electrodes during manual measurments
User controls	20 key tactile, weather proof keyboard with alpha numeric entry keys and function keys. On/off switch. Measure button. LCD night light switch (push to light).
Display	Graphics LCD display (16 lines x 30 characters) with night light.
Power supply, field	12V or 2x12 V DC external power (one or two 12 V batteries), connector on front panel.
Power supply, office	DC power supply
Operating time	Depends on survey conditions and size of battery used. Internal circuitry in auto mode adjusts current to save energy
Operating temperature	-5 to +50ºC
Weight	10.9 kg (24 lb.)
Dimensions	Width 184 mm (7.25"), length 406 mm (16") and height 273 mm (10.75”)

Appendix C: Extended Dipole-Dipole Array

The extended dipole-dipole array provides extended data coverage of the standard dipole-dipole array. The electrode configuration for dipole-dipole is shown below, where the current electrodes (A and B) and potential electrodes (M and N) are equivalently spaced by "a", and separated by a factor "n" times the spacing "a". A measurement of apparent resistivity can be calculated using the equation below the figure, where V = potential difference (V), I = current (Amp), and ρ_A = apparent resistivity (Ohm-m).

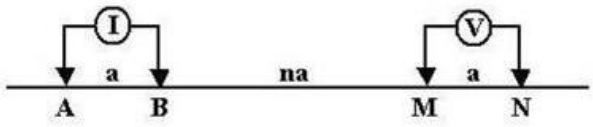

$$\rho_A = \frac{V}{I}\pi\, a\, n(n+1)(n+2).$$

Penetration depth of the extended dipole-dipole array (measurement locations shown below) is approximately 14 times the electrode spacing, which is equivalent to 70m using 5m electrode spacing, but is also dependent on: (1) the actual distribution of subsurface resistivity, and (2) the best achievable contact resistance values between the electrodes and the ground. The figure below shows the measurement locations (in pseudo depth) for an extended dipole-dipole array using 84 surface electrodes.

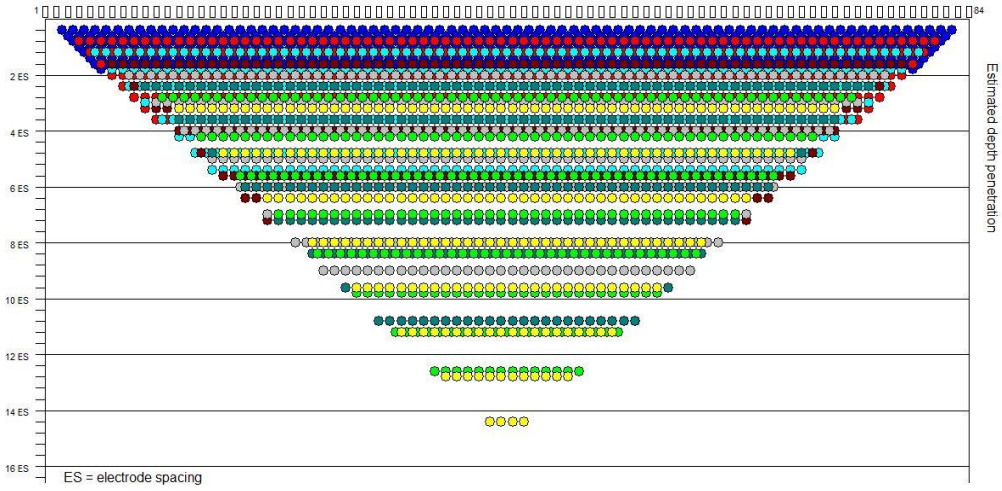

Appendix D: Data Misfit Statistics

(A)

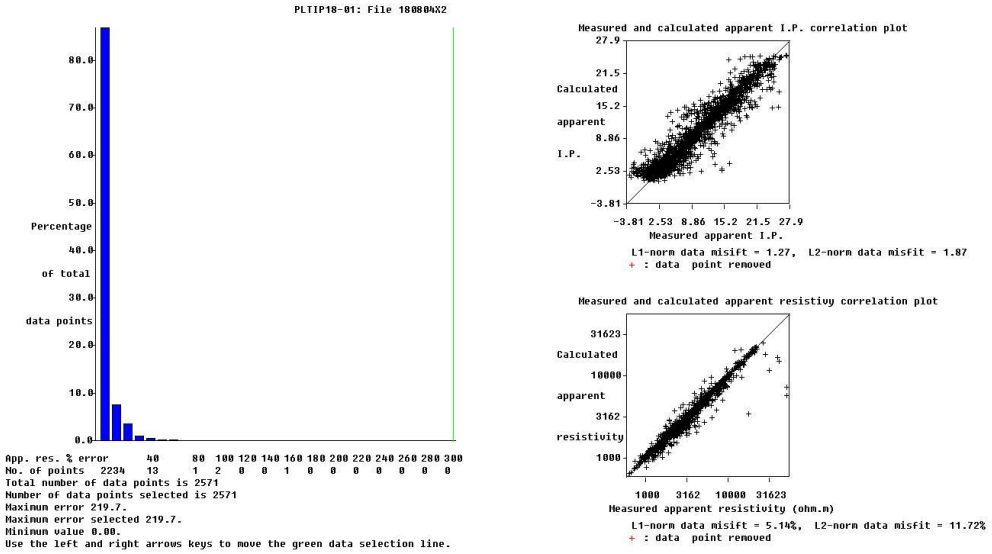

(B)

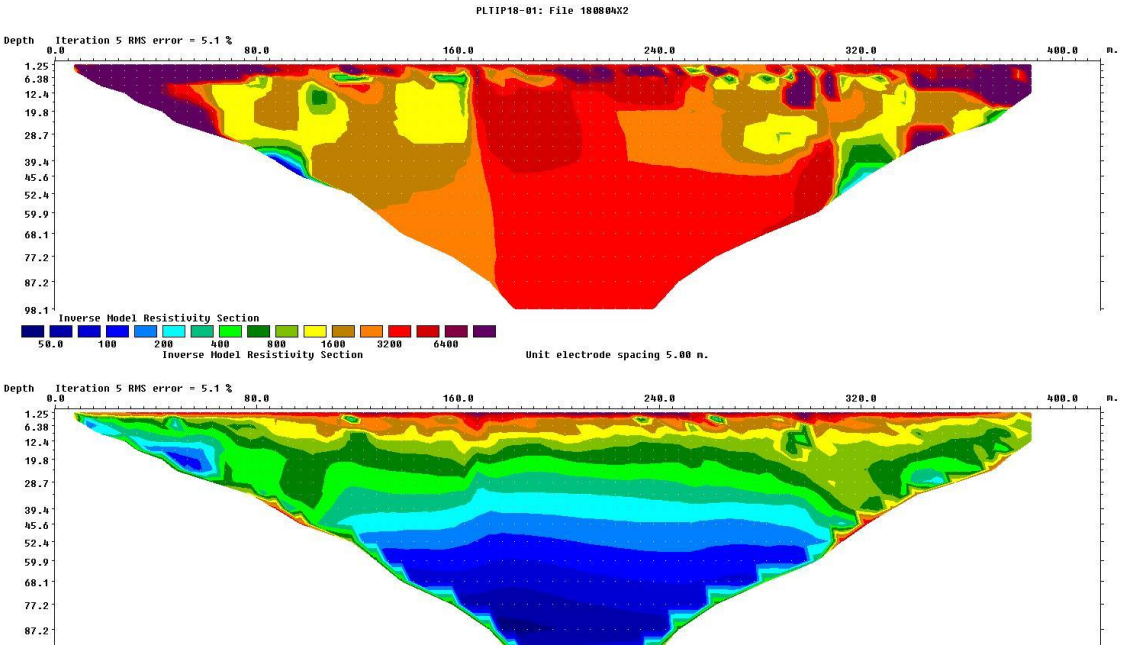

Figure D-1*: PLTIP18-01 data misfit statistics. (**A**) Correlation plots showing distribution of data point error percentage, and calculated vs. measurement apparent resistivity (Ohm-m) and chargeability (ms). (**B**) Sensitivity of inverted resistivity section.*

(A)

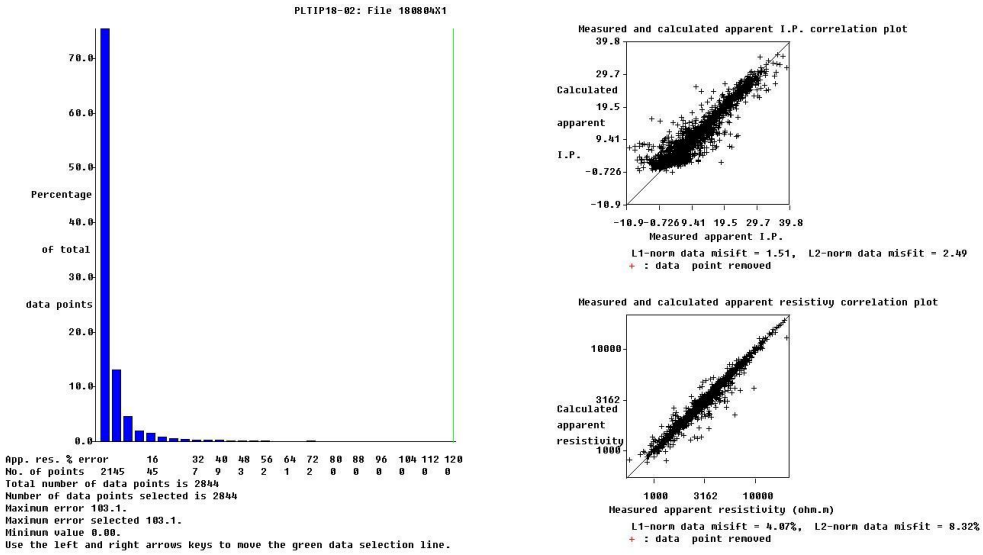

(B)

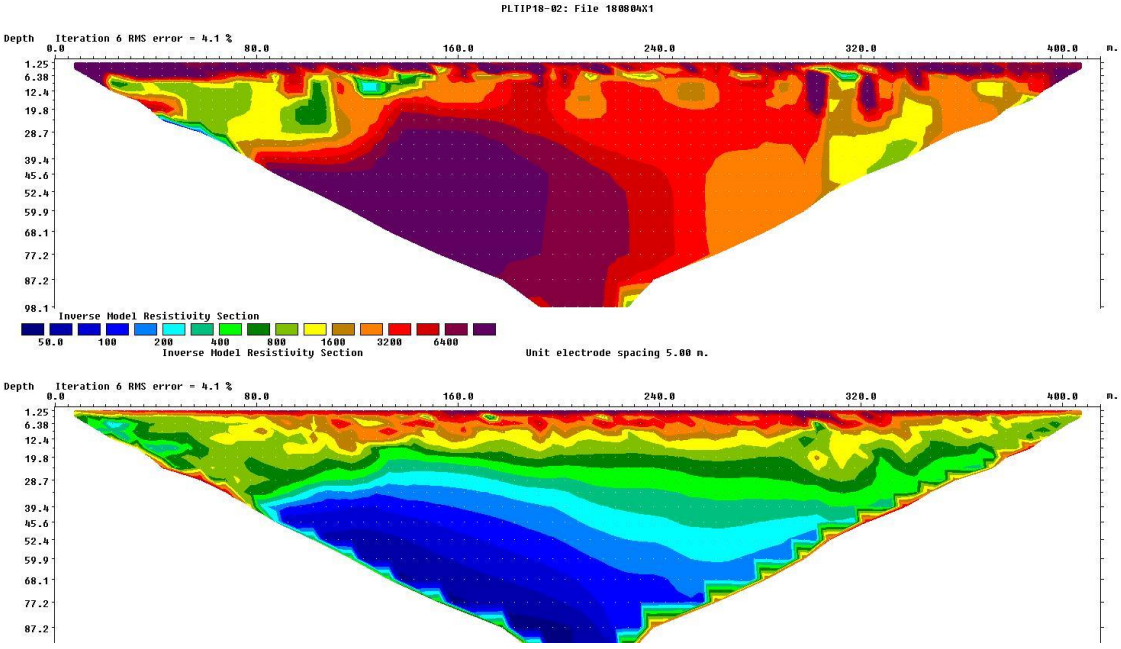

***Figure D-2**: PLTIP18-02 data misfit statistics. (**A**) Correlation plots showing distribution of data point error percentage, and calculated vs. measurement apparent resistivity (Ohm-m) and chargeability (ms). (**B**) Sensitivity of inverted resistivity section.*

(A)

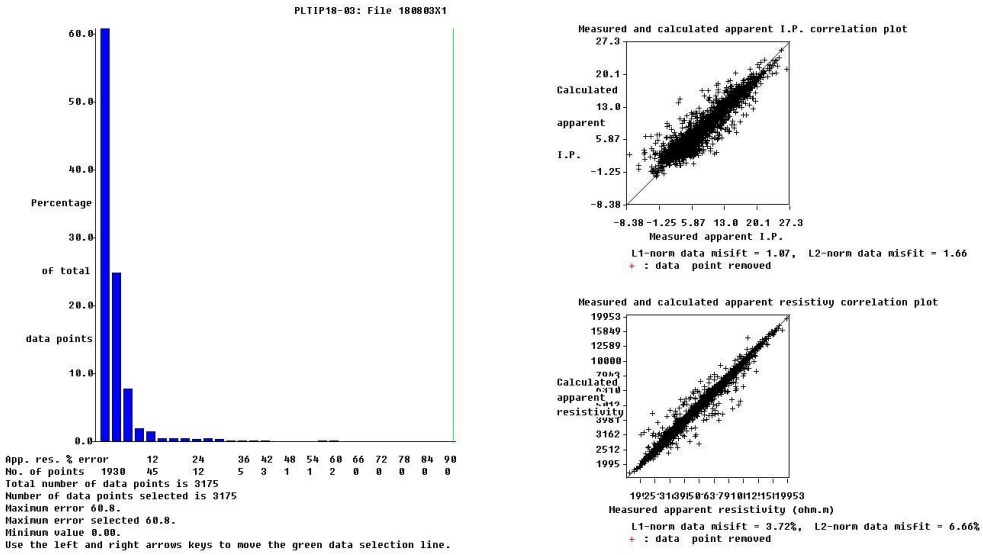

(B)

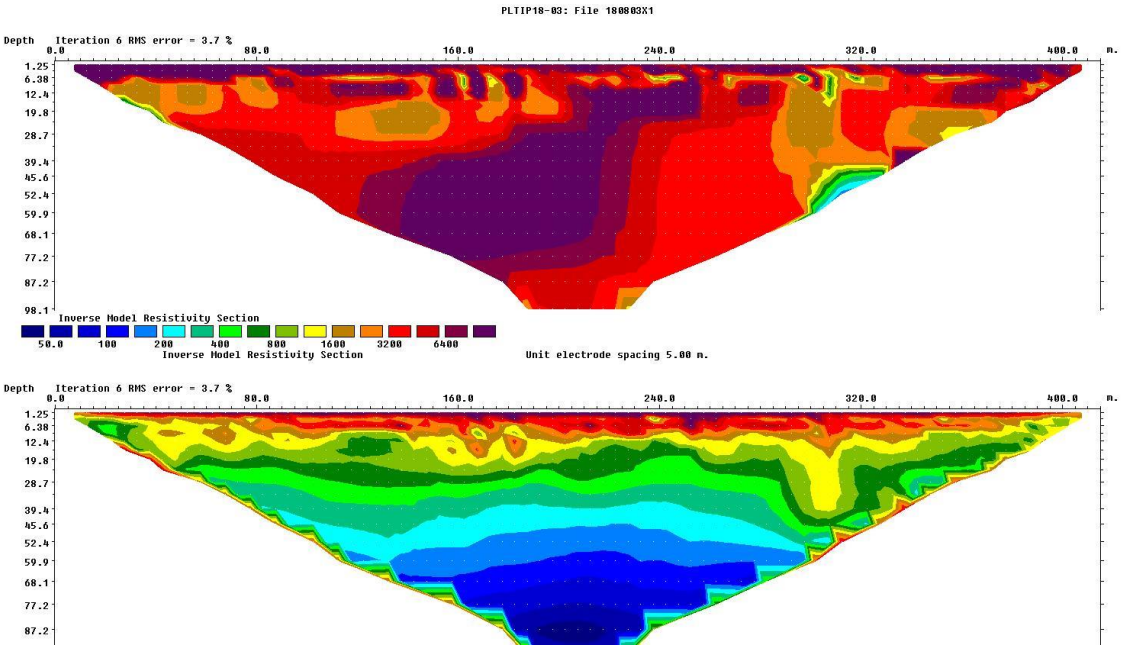

Figure D-3*: PLTIP18-03 data misfit statistics. (**A**) Correlation plots showing distribution of data point error percentage, and calculated vs. measurement apparent resistivity (Ohm-m) and chargeability (ms). (**B**) Sensitivity of inverted resistivity section.*

(A)

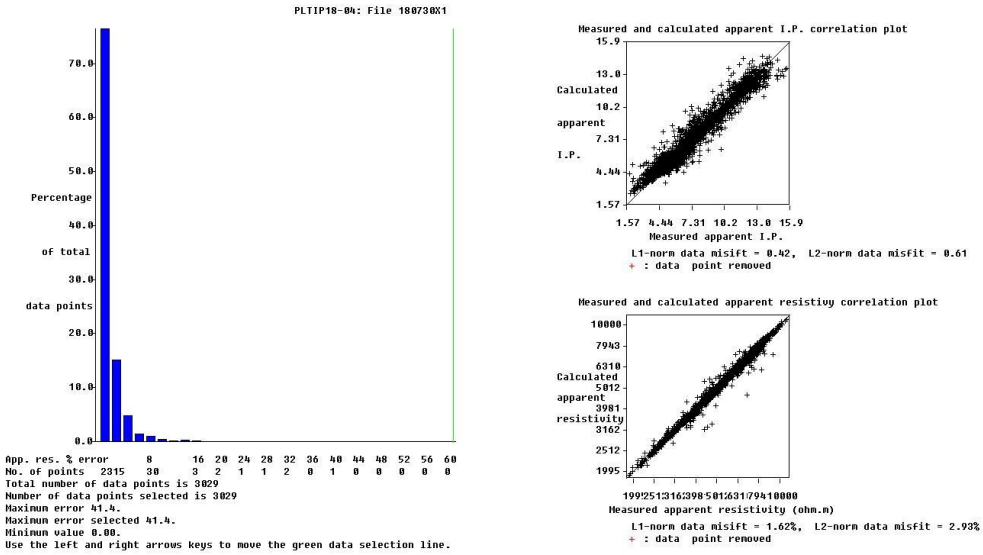

(B)

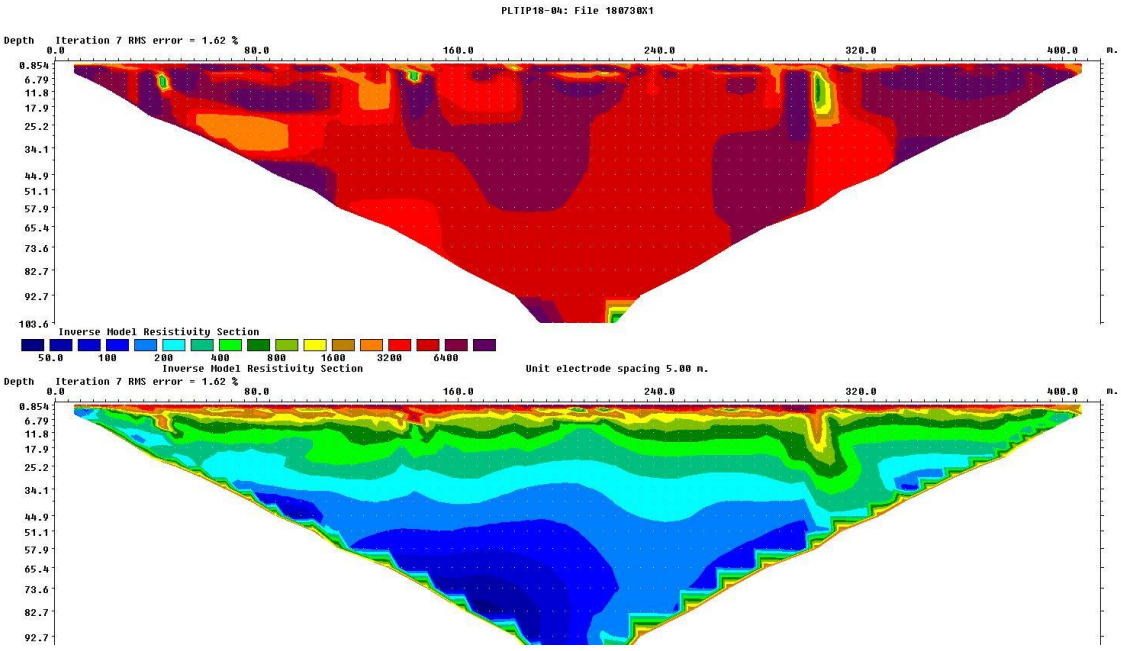

Figure D-4*: PLTIP17-04 data misfit statistics. (**A**) Correlation plots showing distribution of data point error percentage, and calculated vs. measurement apparent resistivity (Ohm-m) and chargeability (ms). (**B**) Sensitivity of inverted resistivity section.*

(A)

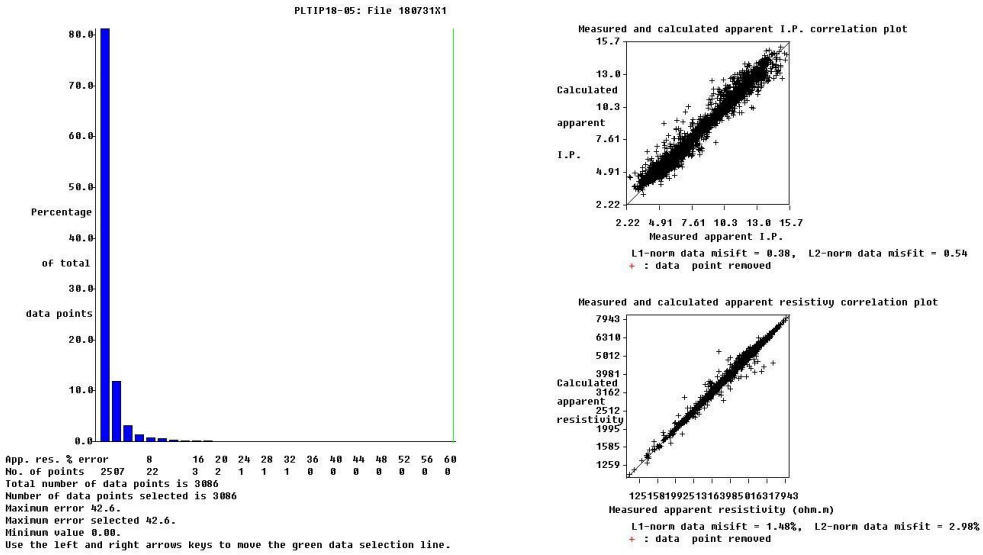

(B)

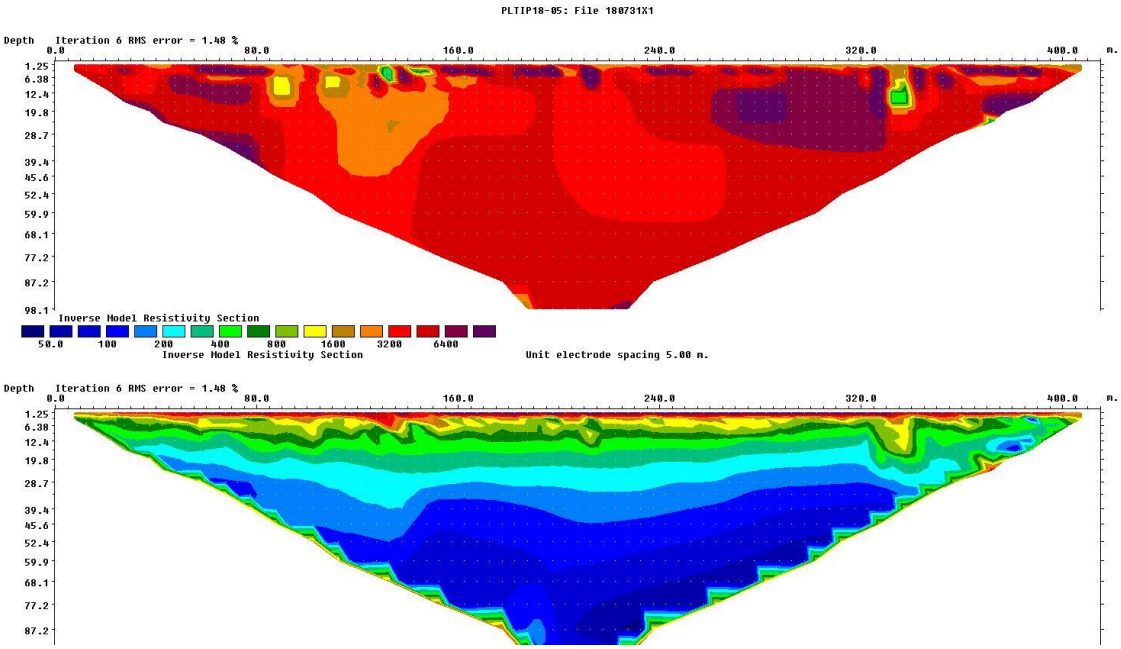

Figure D-5*: PLTIP18-05 data misfit statistics. (**A**) Correlation plots showing distribution of data point error percentage, and calculated vs. measurement apparent resistivity (Ohm-m) and chargeability (ms). (**B**) Sensitivity of inverted resistivity section.*

(A)

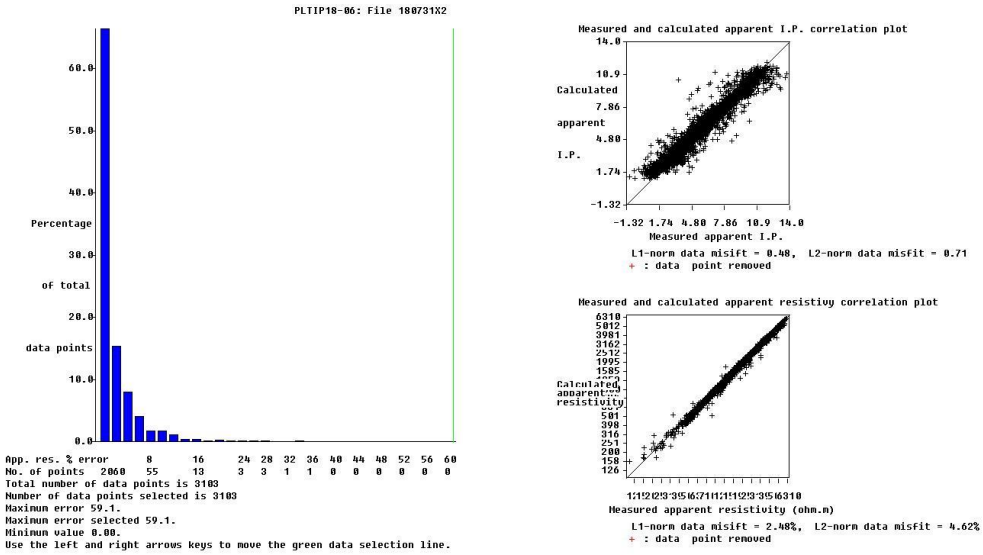

(B)

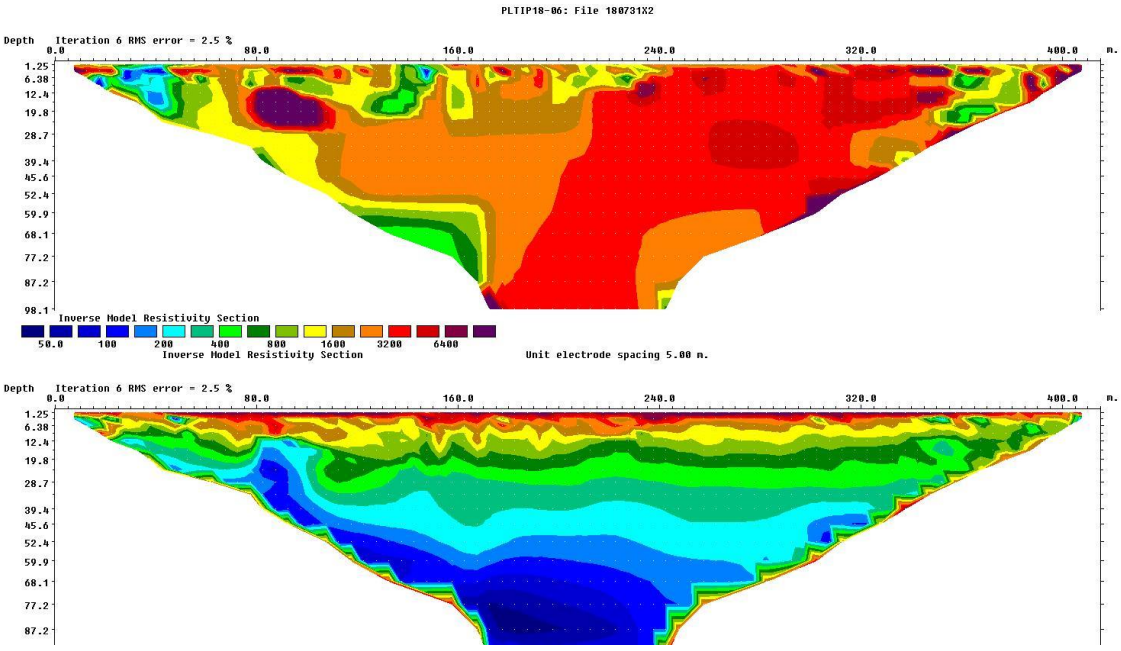

Figure D-6*: PLTIP18-06 data misfit statistics. (**A**) Correlation plots showing distribution of data point error percentage, and calculated vs. measurement apparent resistivity (Ohm-m) and chargeability (ms). (**B**) Sensitivity of inverted resistivity section.*

(A)

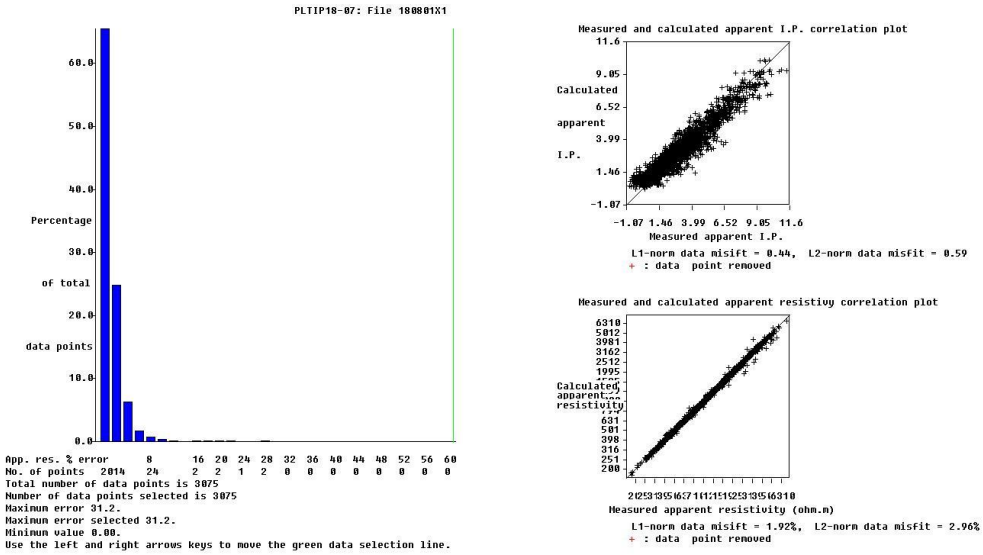

(B)

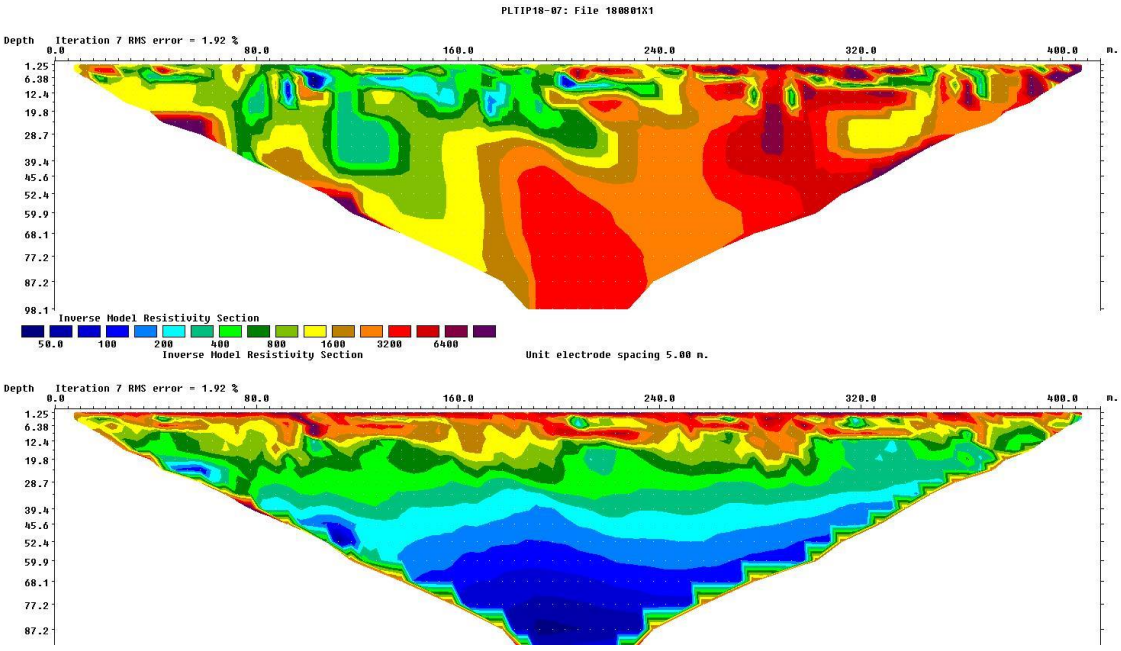

Figure D-7*: PLTIP18-07 data misfit statistics. (**A**) Correlation plots showing distribution of data point error percentage, and calculated vs. measurement apparent resistivity (Ohm-m) and chargeability (ms). (**B**) Sensitivity of inverted resistivity section.*

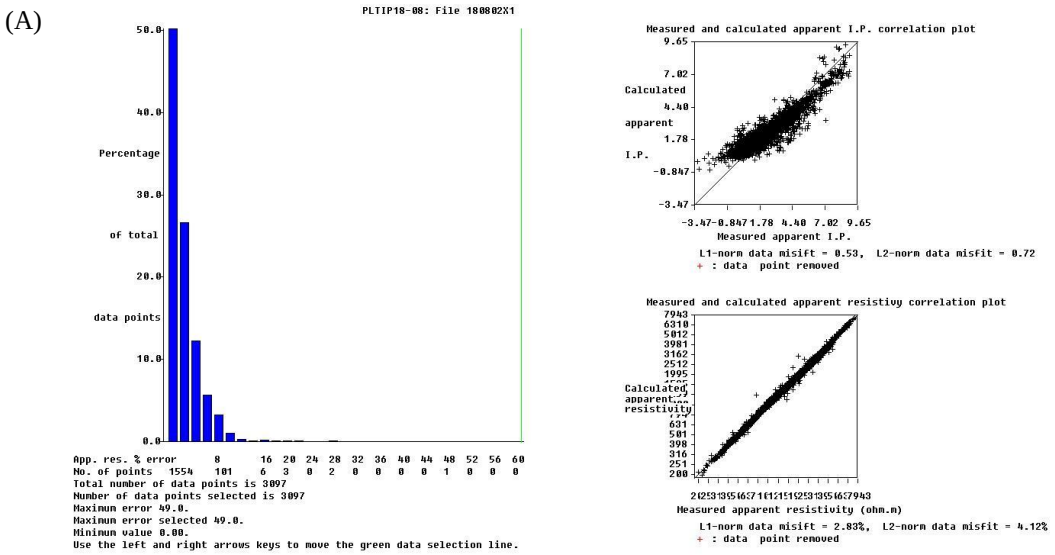

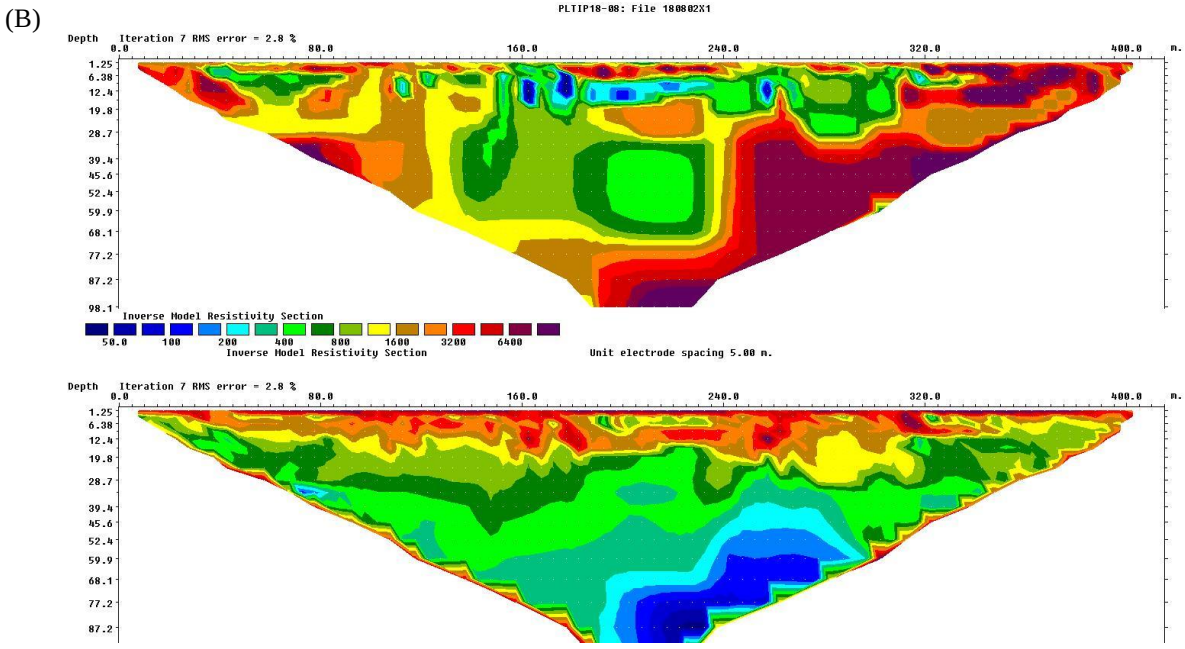

Figure D-8*: PLTIP18-08 data misfit statistics. (**A**) Correlation plots showing distribution of data point error percentage, and calculated vs. measurement apparent resistivity (Ohm-m) and chargeability (ms). (**B**) Sensitivity of inverted resistivity section.*

(A)

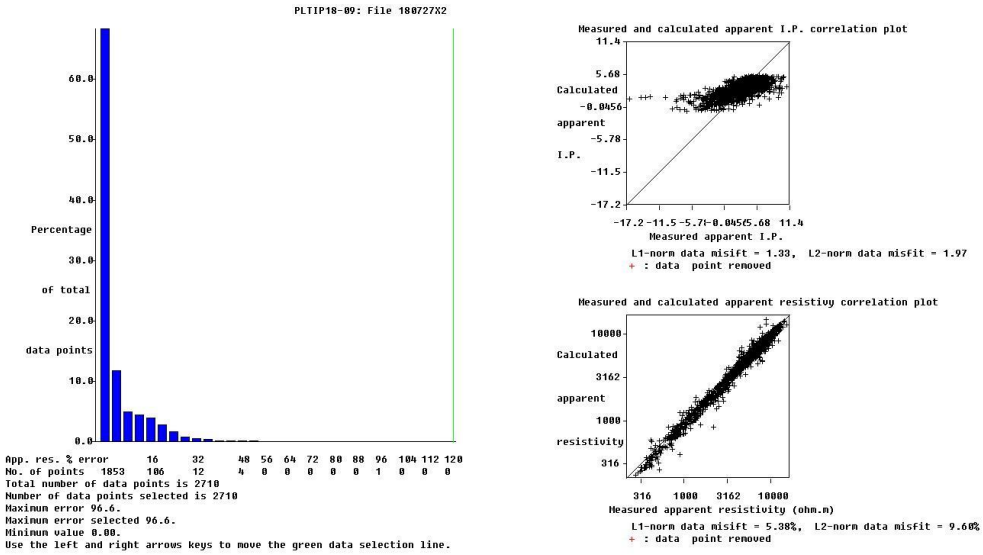

(B)

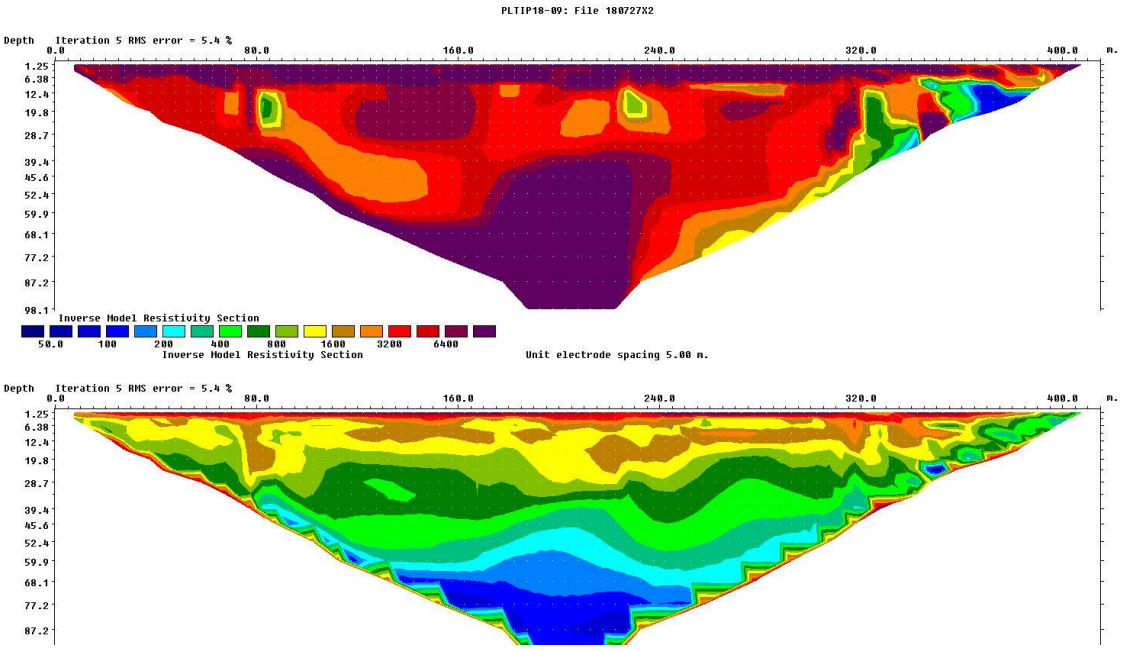

Figure D-9*: PLTIP18-09 data misfit statistics. (**A**) Correlation plots showing distribution of data point error percentage, and calculated vs. measurement apparent resistivity (Ohm-m) and chargeability (ms). (**B**) Sensitivity of inverted resistivity section.*

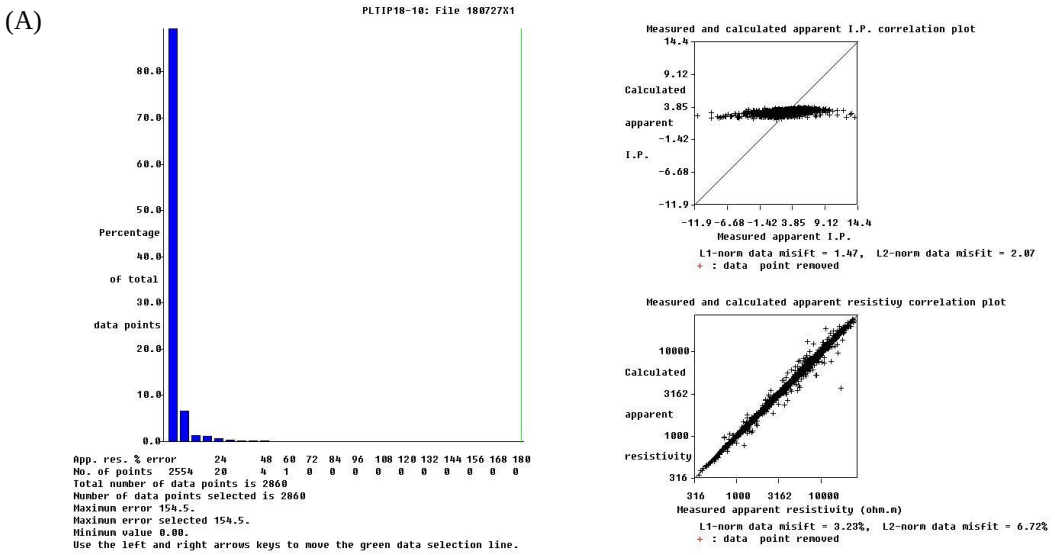

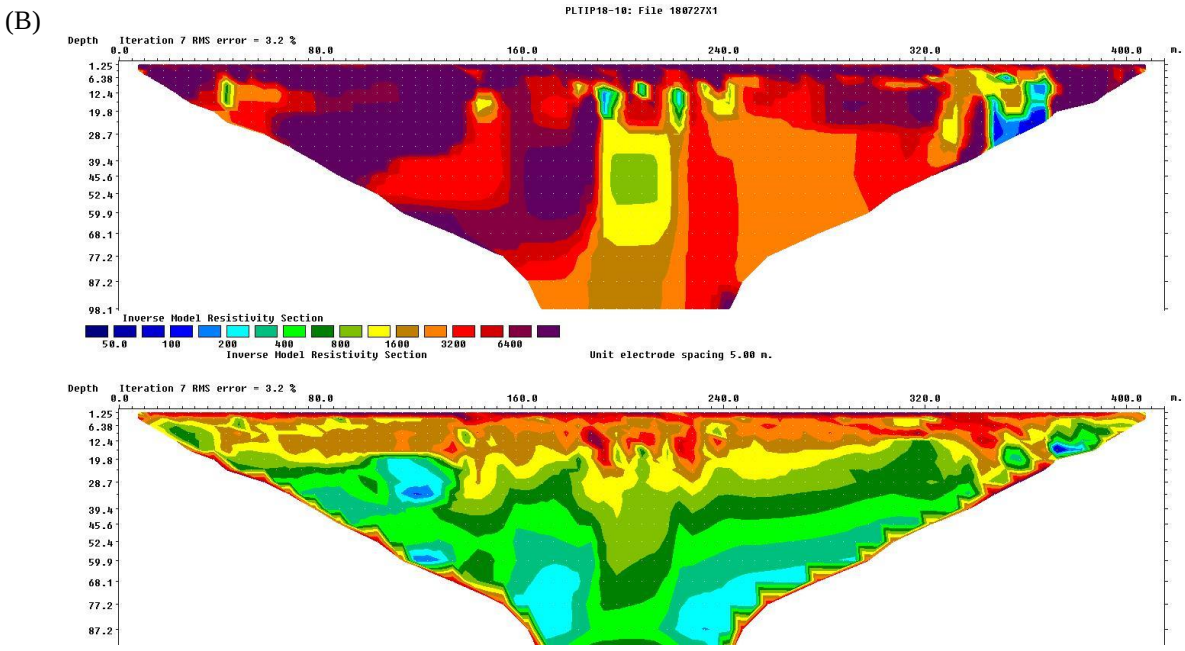

***Figure D-10**: PLTIP18-10 data misfit statistics. (**A**) Correlation plots showing distribution of data point error percentage, and calculated vs. measurement apparent resistivity (Ohm-m) and chargeability (ms). (**B**) Sensitivity of inverted resistivity section.*

(A)

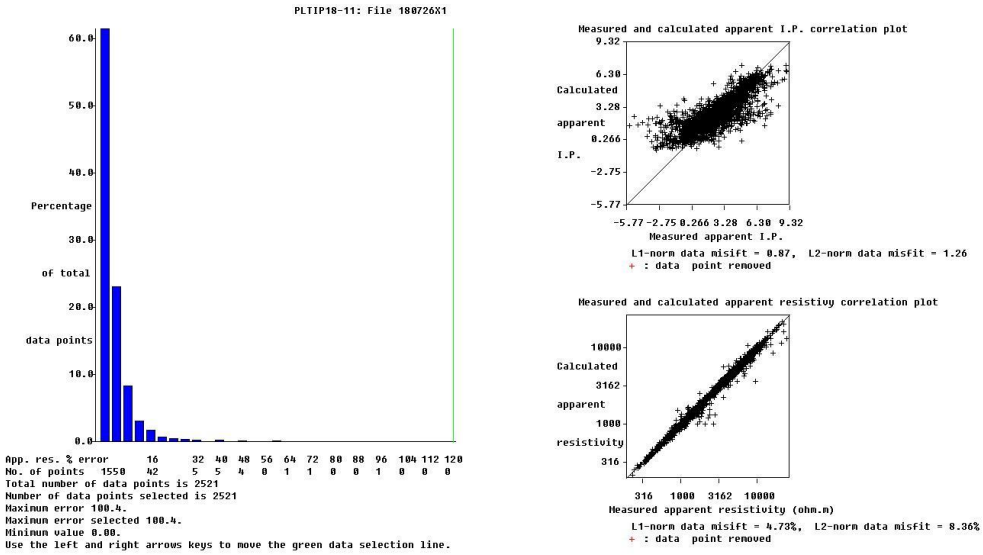

(B)

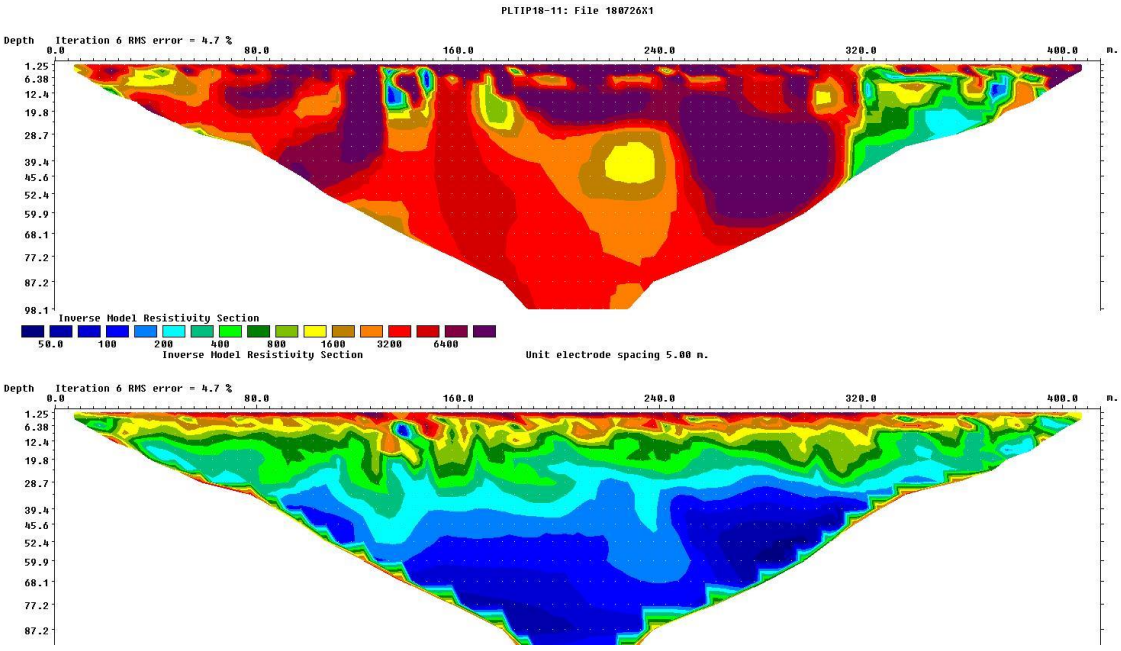

Figure D-11*: PLTIP18-11 data misfit statistics. (**A**) Correlation plots showing distribution of data point error percentage, and calculated vs. measurement apparent resistivity (Ohm-m) and chargeability (ms). (**B**) Sensitivity of inverted resistivity section.*

(A)

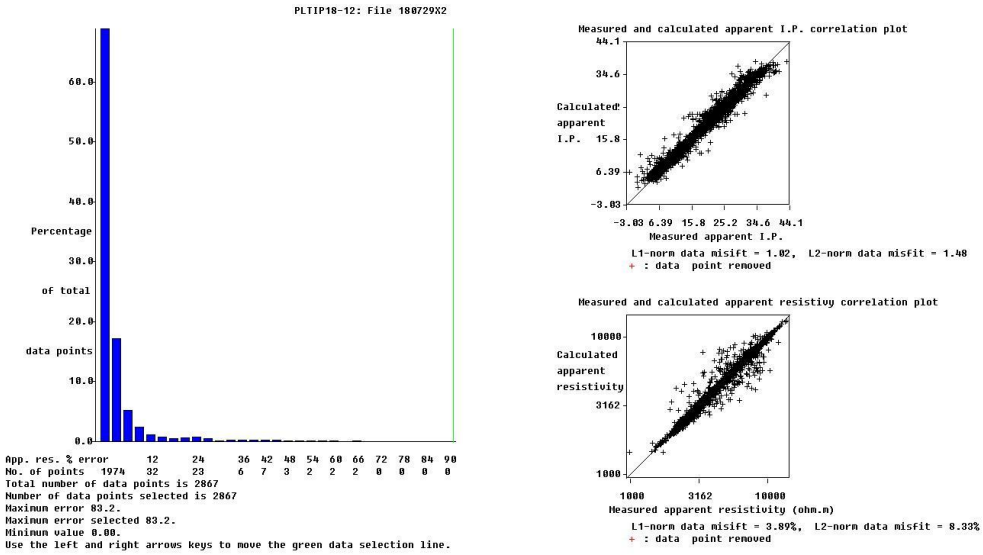

(B)

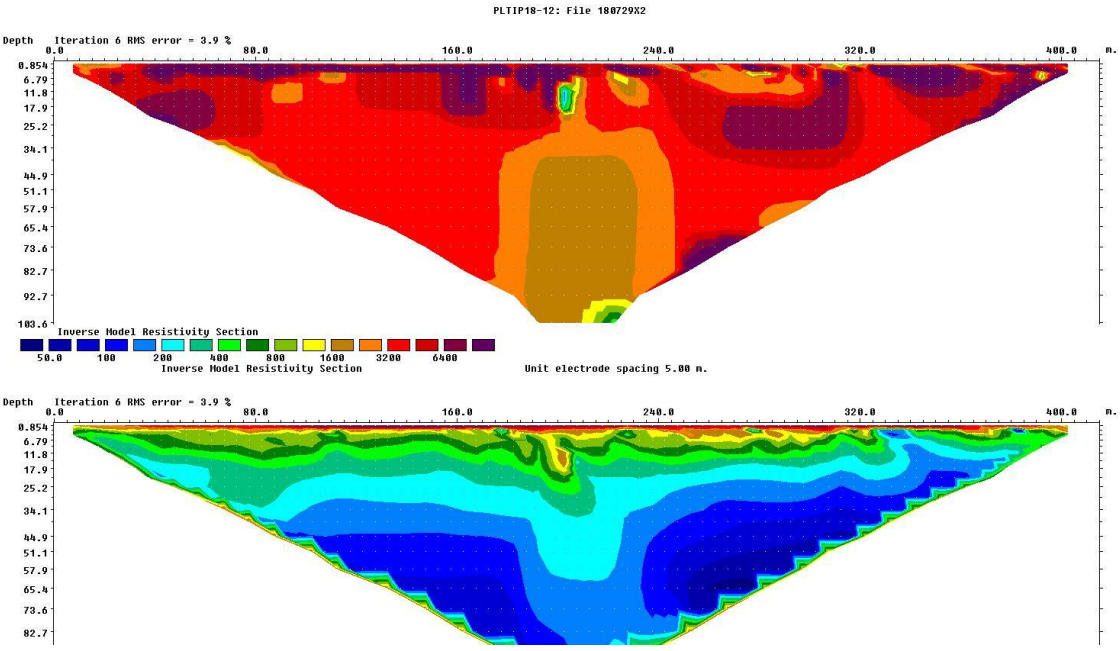

***Figure D-12**: PLTIP18-12 data misfit statistics. (**A**) Correlation plots showing distribution of data point error percentage, and calculated vs. measurement apparent resistivity (Ohm-m) and chargeability (ms). (**B**) Sensitivity of inverted resistivity section.*

(A)

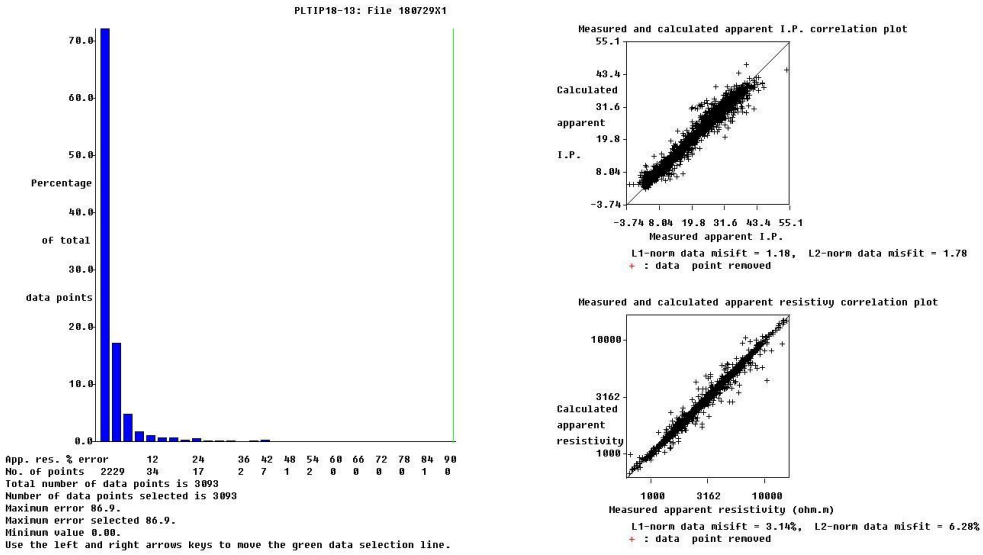

(B)

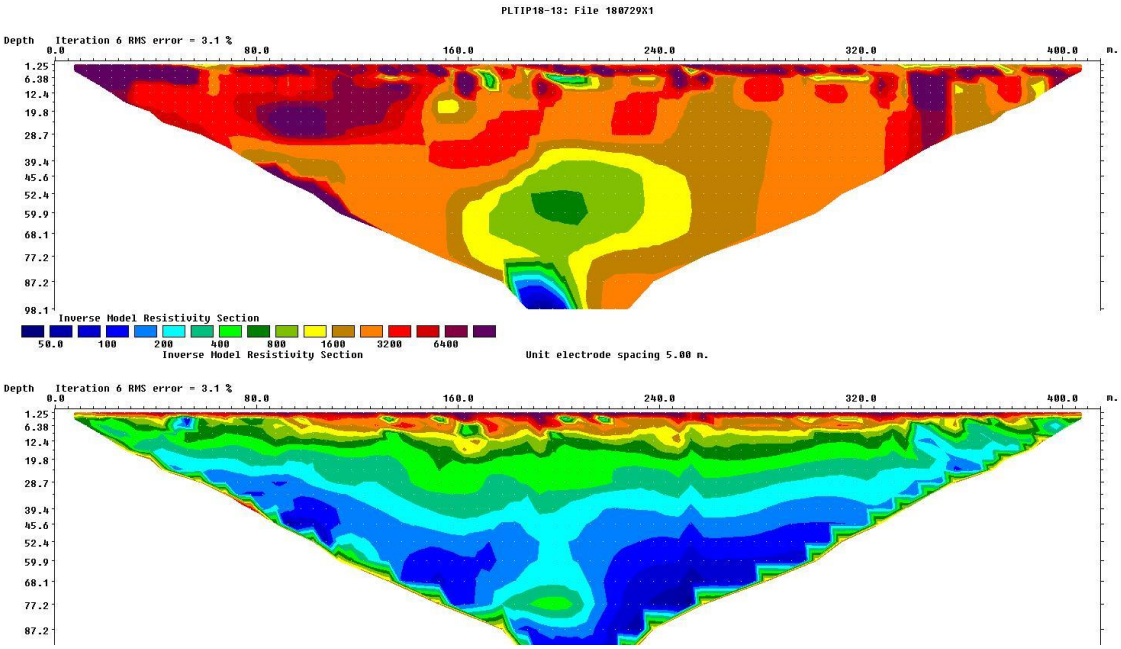

***Figure D-13**: PLTIP18-13 data misfit statistics. (**A**) Correlation plots showing distribution of data point error percentage, and calculated vs. measurement apparent resistivity (Ohm-m) and chargeability (ms). (**B**) Sensitivity of inverted resistivity section.*

(A)

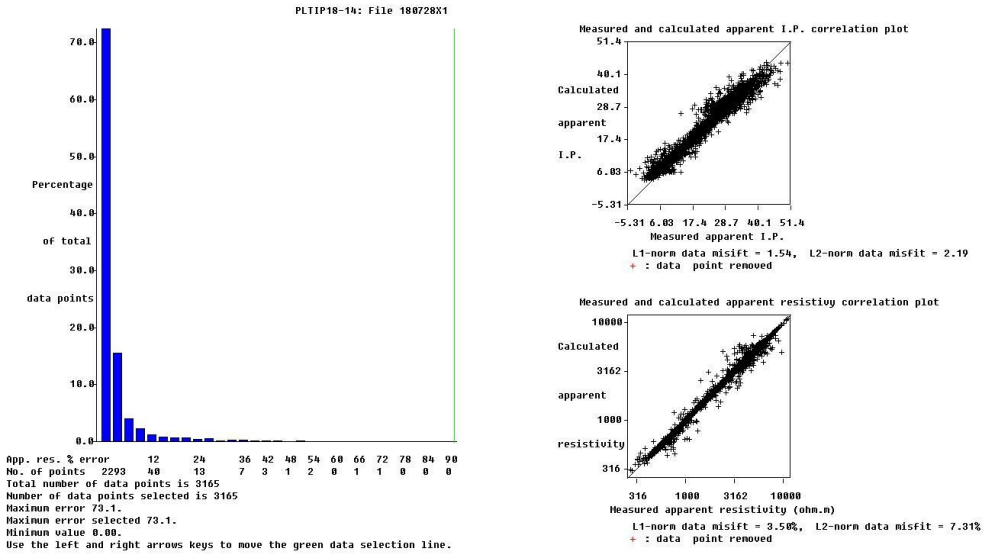

(B)

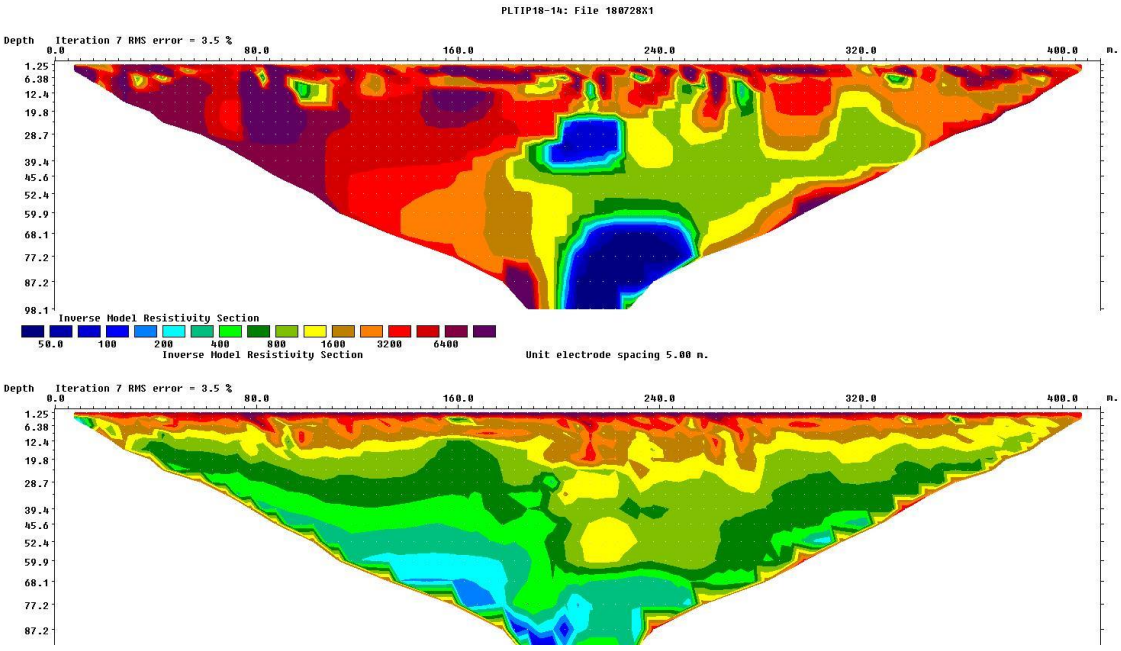

***Figure D-14**: PLTIP18-14 data misfit statistics. (**A**) Correlation plots showing distribution of data point error percentage, and calculated vs. measurement apparent resistivity (Ohm-m) and chargeability (ms). (**B**) Sensitivity of inverted resistivity section.*